REPORT DOCUMENTATION PAGE	Form Approved OMB NO. 0704-0188

Public reporting burden for this collection of information is estimated to average 1 hour per response, including the time for reviewing instructions, searching existing data sources, gathering and maintaining the data needed, and completing and reviewing the collection of information. Send comment regarding this burden estimates or any other aspect of this collection of information, including suggestions for reducing this burden, to Washington Headquarters Services, Directorate for information Operations and Reports, 1215 Jefferson Davis Highway, Suite 1204, Arlington, VA 22202-4302, and to the Office of Management and Budget, Paperwork Reduction Project (0704-0188), Washington, DC 20503.

1. AGENCY USE ONLY (Leave blank)	2. REPORT DATE 6/24/99	3. REPORT TYPE AND DATES COVERED Final Report 9/1/97 – 3/31/99

4. TITLE AND SUBTITLE	5. FUNDING NUMBERS
DEMONSTRATION OF A SHORT WAVELENGTH CHEMICAL LASER	DAAG55-97-1-0397

6. AUTHOR(S)

James L. Gole

7. PERFORMING ORGANIZATION NAMES(S) AND ADDRESS(ES)	8. PERFORMING ORGANIZATION REPORT NUMBER
Georgia Tech Research Corporation Georgia Institute of Technology Office of Contract Administration Atlanta, Georgia 30332-0430	

9. SPONSORING / MONITORING AGENCY NAME(S) AND ADDRESS(ES)	10. SPONSORING / MONITORING AGENCY REPORT NUMBER
U.S. Army Research Office P.O. Box 12211 Research Triangle Park,, NC 27709-2211	ARO 37668.1-PH

11. SUPPLEMENTARY NOTES

The views, opinions and/or findings contained in this report are those of the author(s) and should not be construed as an official Department of the Army position, policy or decision, unless so designated by other documentation.

12a. DISTRIBUTION / AVAILABILITY STATEMENT	12b. DISTRIBUTION CODE
Approved for public release; distribution unlimited.	

13. ABSTRACT (Maximum 200 words)

Experiments to demonstrate a short wavelength chemical laser based on atomic sodium have been performed. The metastable states of SiO generated using the Si–N_2O reaction have been used to energy transfer pump a Na atom amplifier at 569 nm (Na $4d^2D \rightarrow$ Na$3p^2P+h\nu$ (569 nm)). Using this gain medium in a full vacuum cavity constructed following the design of the HF overtone system at the University of Illinois, Urbana, we have pursued and are continuing experiments to demonstrate lasing at 569 nm.

19991102 136

14. SUBJECT TERMS		15. NUMBER IF PAGES
		16. PRICE CODE

17. SECURITY CLASSIFICATION OR REPORT UNCLASSIFIED	18. SECURITY CLASSIFICATION OF THIS PAGE UNCLASSIFIED	19. SECURITY CLASSIFICATION OF ABSTRACT UNCLASSIFIED	20. LIMITATION OF ABSTRACT UL

NSN 7540-01-280-5500

Standard Form 298 (Rev. 2-89)
Prescribed by ANSI Std. 239-18
298-102

Demonstration of a Short Wavelength Chemical Laser

Final Progress Report

James L. Gole

June 24, 1999

U. S. ARMY RESEARCH OFFICE

DAAG55-97-1-0397

Georgia Institute of Technology
School of Physics
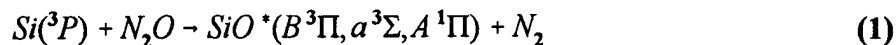Atlanta, GA 30332-0430

Approved for Public Release;

Distribution Unlimited.

Table of Contents

Background

The metastable states of the SiO molecule formed in the reaction,

$$Si(^3P) + N_2O \rightarrow SiO\,^*(B\,^3\Pi, a\,^3\Sigma, A\,^1\Pi) + N_2 \qquad (1)$$

where the metastable triplet states dominate the product formation, possess an energy of approximately 3.5 eV and a lifetime of order 10 ms.[1] This suggests the SiO metastables as potential donors for an energy transfer based visible laser system operative on the pumping of select atomic transitions.

In order to develop a visible chemical laser, we require the creation of a visible chemical laser amplifier and the demonstration of gain on transitions in the visible region of the spectrum evaluated using zero power gain measurements. The high precision gain measurements outlined in Appendix A of this report demonstrate that the sequence
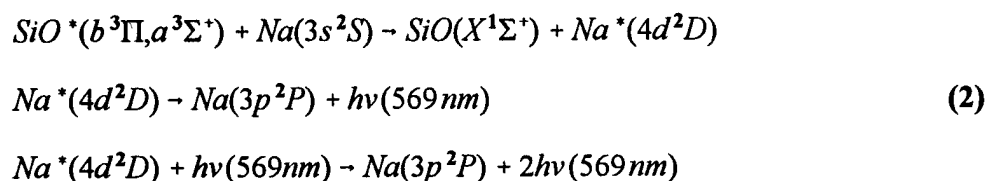
$$SiO\,^*(b\,^3\Pi, a\,^3\Sigma^+) + Na(3s\,^2S) \rightarrow SiO(X\,^1\Sigma^+) + Na\,^*(4d\,^2D)$$

$$Na\,^*(4d\,^2D) \rightarrow Na(3p\,^2P) + h\nu(569\,nm) \qquad (2)$$

$$Na\,^*(4d\,^2D) + h\nu(569\,nm) \rightarrow Na(3p\,^2P) + 2h\nu(569\,nm)$$

forms an energy transfer system which represents a viable chemical laser candidate based on amplification at 569 nm.[2] Based on the analysis of the experimental results outlined in Appendix A, a conservatively estimated gain coefficient of 0.8 to 1.5 x 10^{-3} cm^{-1} at 569 nm, and the analytical estimates given in Appendix B, we have constructed an appropriate full cavity vacuum mirror mount configuration in order to provide a lasing (oscillator) demonstration. This report describes our progress in these ongoing studies.

1

The sodium atom represents one of the best candidates for energy transfer from metastable SiO molecules. The $4d^2D$ level of sodium, which is not accessible via optical pumping from the ground electronic state, possesses several near resonances with the $SiO^*(b^3\Pi)$ state (Table I). Near resonant energy transfer pumping to this level, with subsequent decay and potential lasing, is illustrated in the Sequence (2) above. The relevant energy levels are outlined in Figure 1. In the Sequence (2) the $3p^2P$ level represents the terminal laser level which, as it decays rapidly to the $3s^2S$ ground state (the sodium D-line transition with $\tau_{rad} \sim 15$ ns),[3] facilitates the creation of an inversion. The decay from the $4d^2D$ level (with $\tau_{rad} \sim 80$ ns)[4] suggests the possibility for a high duty cycle. In fact, evidence for continuous amplification has been reported by Shen et al.[2,5] Using the Einstein A coefficients for the $4d^2D$ - $3p^2P$ transitions given in Table II, we can estimate a saturation intensity[6] of $6W\text{-}cm^{-2}$ for a laser operating at 569 nm (at 500 K), suggesting that the SiO - Na^* energy transfer sequence represents a viable route to create a visible chemical laser oscillator.

Overview of System

Because we are attempting to demonstrate lasing in a low-gain system, it is appropriate that we operate with a vacuum mirror mount configuration. The construction of this system has followed closely that already used to study the HF overtone system at the U. of Illinois, Urbana albeit with the necessity of a more complex Si source-oxidation reaction - SiO metastable - Na energy transfer zone to produce the desired population inversion in atomic sodium. The overall system, pictured in front and side view in Figures 2 and 3 and diagramed schematically in Figure 4, has required the construction of vacuum boxes, surrounding a central reaction-energy transfer
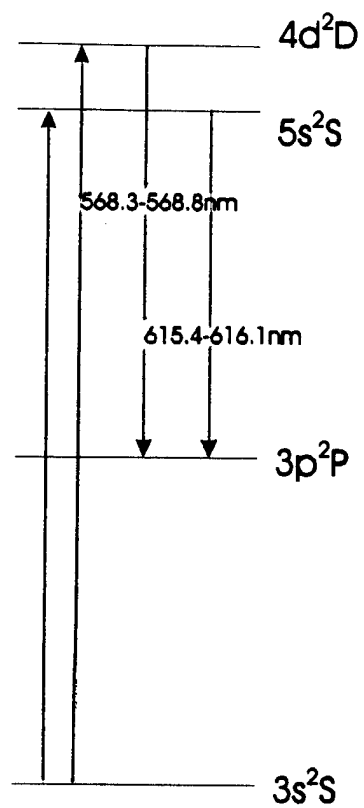
2

Figure 1

Simplified level diagram for sodium depicting
levels relevant for proposed laser.

Table I
Near resonances of SiO*(b³Π - X¹Σ⁺) with Na 3s²S-4d²D pump transition

Upper Atomic Level	SiO(v', v'') b - X	$\Delta E(cm^{-1})$[a]
Na 4d²D$_{5/2,3/2}$	(1,0)	294
	(2,1)	45
	(3,2)	-209

a. Approximate value of molecular energy level minus atomic energy level. Positive denotes exothermic energy transfer.

Table II
Spontaneous emission rates, degeneracy factors and energy increments for Na 4d²D transition (from *Handbook of Chemistry and Physics*, 64th Ed.)

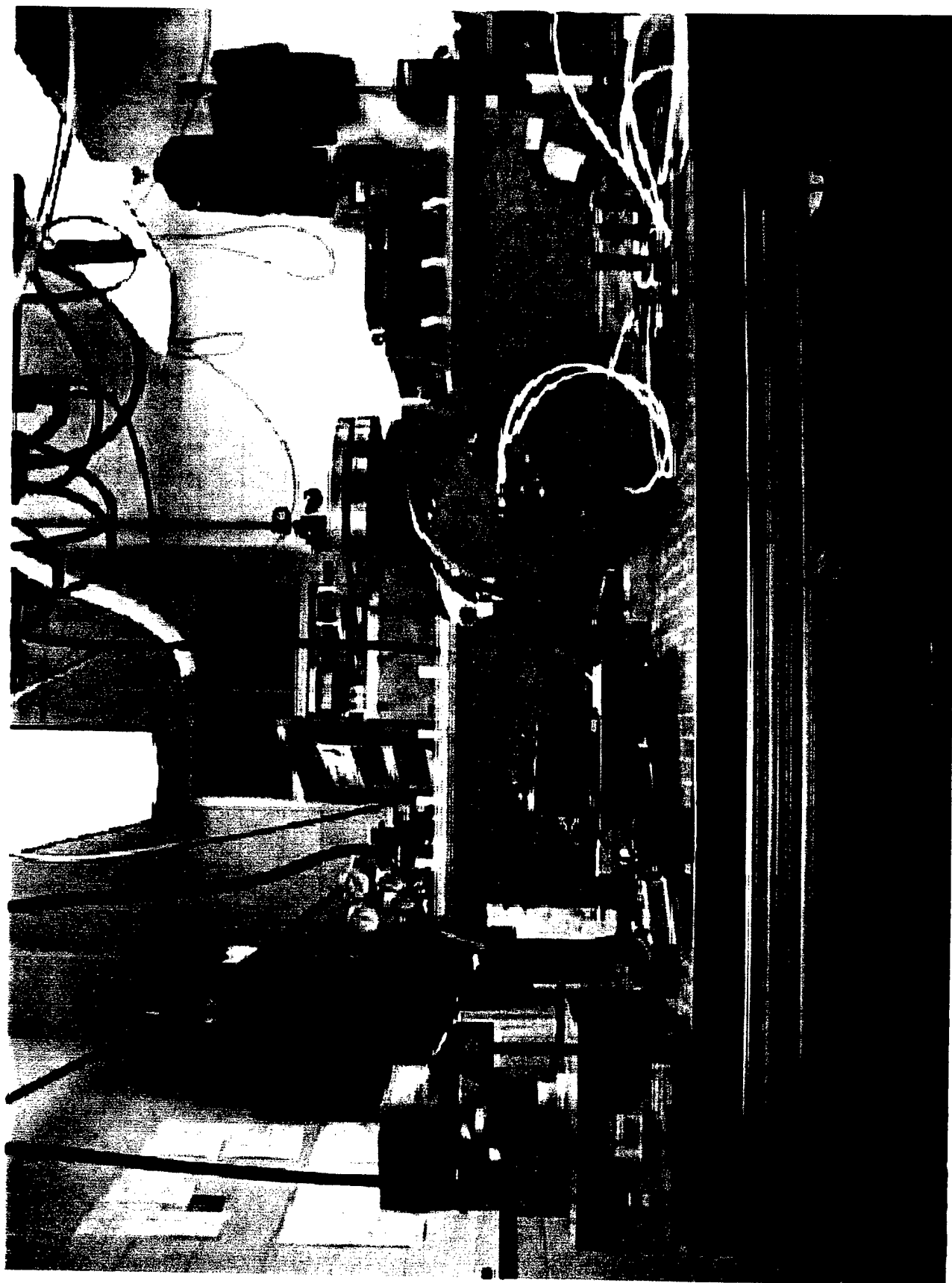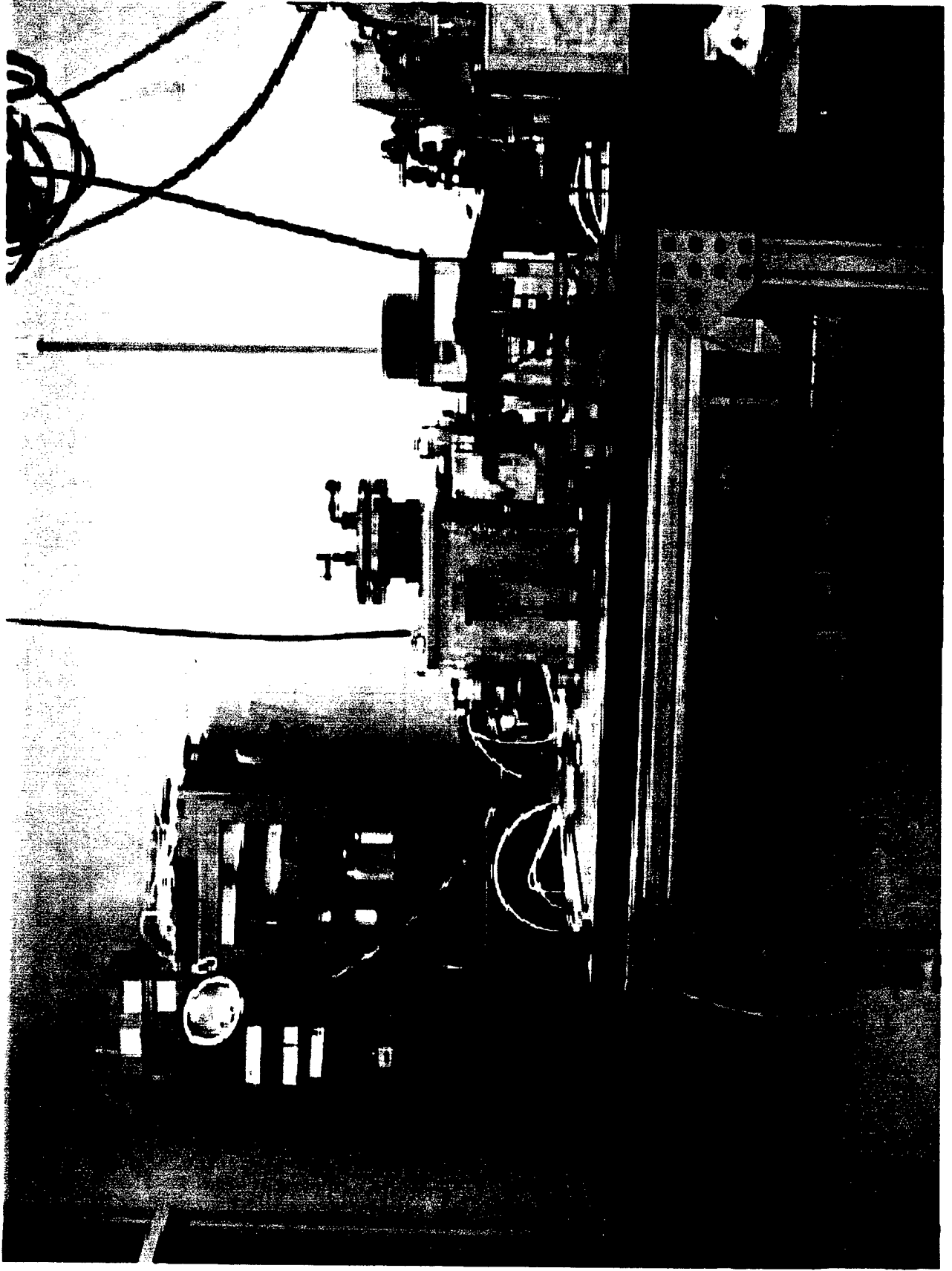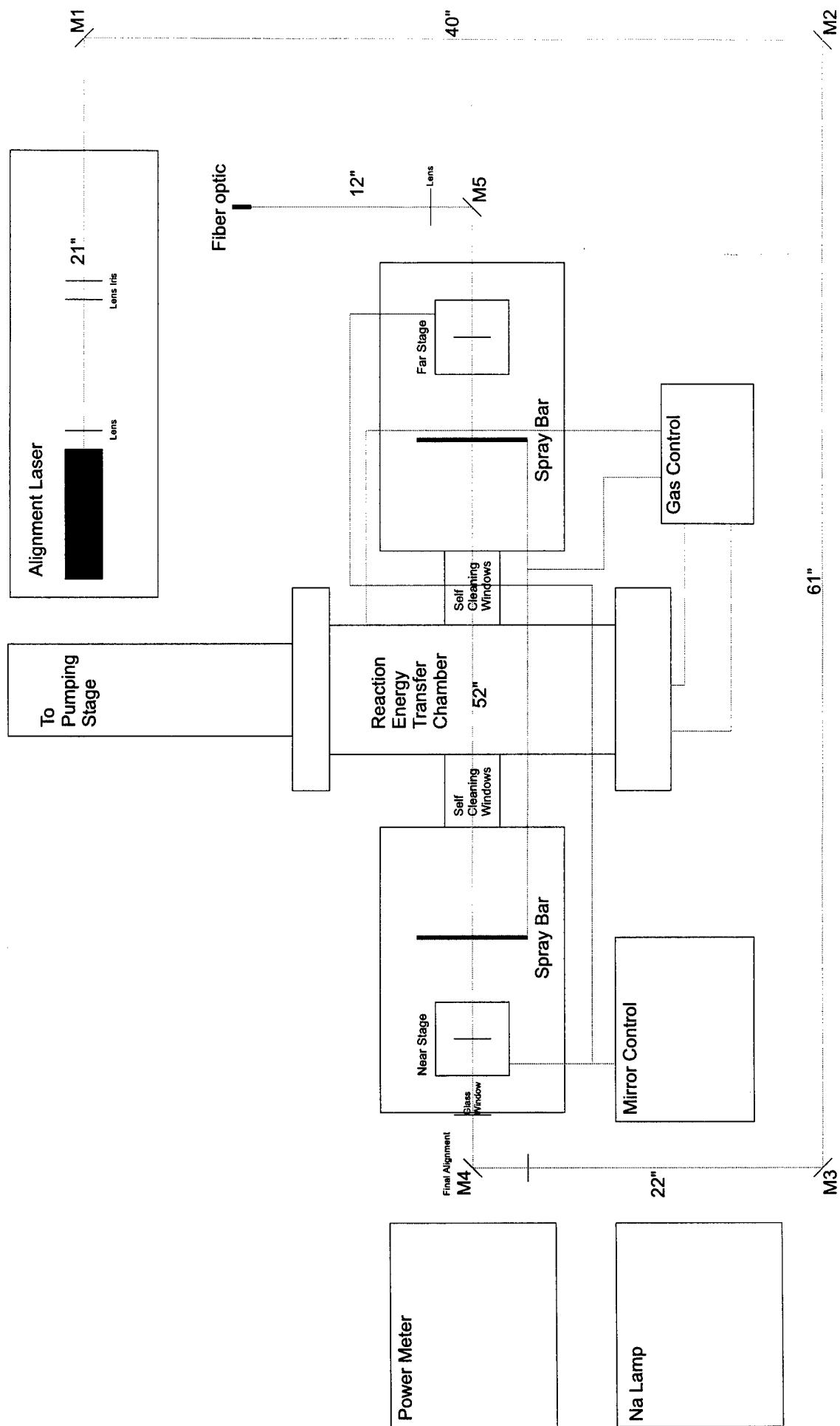| Transition	Energy(cm⁻¹)	A value (10⁷ s⁻¹)	g_u	g_e
4d²D$_{5/2}$-3p²P$_{3/2}$	17575.375	1.2	6	4
4d²D$_{3/2}$-3p²P$_{3/2}$	17575.41	0.21	4	4
4d²D$_{3/2}$-3p²P$_{1/2}$	17592.606	1.03	4	2

Figure 2

Figure 3

Figure 4

chamber (Figures 5 and 6). These chambers contain near and far stage water coded motorized mirror mounts, the mirror mounts being equipped with motor mics (homebuilt remote controllers). The near and far stages are thus constructed into motorized stage assemblies for control and placement (translation) of the resonator mirrors in vacuum. They each consist of motorized horizontal translational stages (Oriel model 16137), vertical translation stages with encoder motor actuators (Oriel model 16618), a motorized gumbaled mirror mount (Oriel model 18160), and a single axis encoder motor controller for the vertical translation stage (Oriel model 18160).

The remaining components of the system consist of associated alignment devices (HeNe laser, custom alignment jigs, mountable pinhole alignment targets), the principal diagnostic power meter detection system (Scientech MC2500, MD10, 36-0203M), and multimode fiber optic cable so as to (1) evaluate stimulated vs. spontaneous emission and (2) allow the determination of the precise components of the light output from the reaction energy transfer zone due to the Sequence (2). The entire configuration pictured and diagramed in Figures 2-4 is mounted on a custom built optical breadboard (Newport-Klinger) and underpinning table (College of Science machine shop) with center opening to accomodate the SiO^*-Na^* reaction-energy transfer vacuum chamber depicted schematically in Figures 5 and 6.

Specifics of Experiments

We are attempting to lase the SiO metastable-sodium energy transfer system using a combination of nominally 99.7% reflective mirrors (Appendix B). The vacuum mirror mount boxes are attached to the ports of the reaction-energy transfer vacuum chamber through self-

Relief Valve

Thermocouple Gauge

18"

SiO Source Oven

Sodium Source Oven

Figure 5

(a)

Silicon Oven Top

Outlet

Reaction System
Alignment Block

Nozzle Array
(cut view)

Sodium and Carrying Gas

N_2O

Carrying Gas (N_2) for silicon

(b)

Water-Cooled   Heat
Brass Jacket Reflector

Tantalum
Heater

Si

Graphite
Crucible

Zirconia
Felt

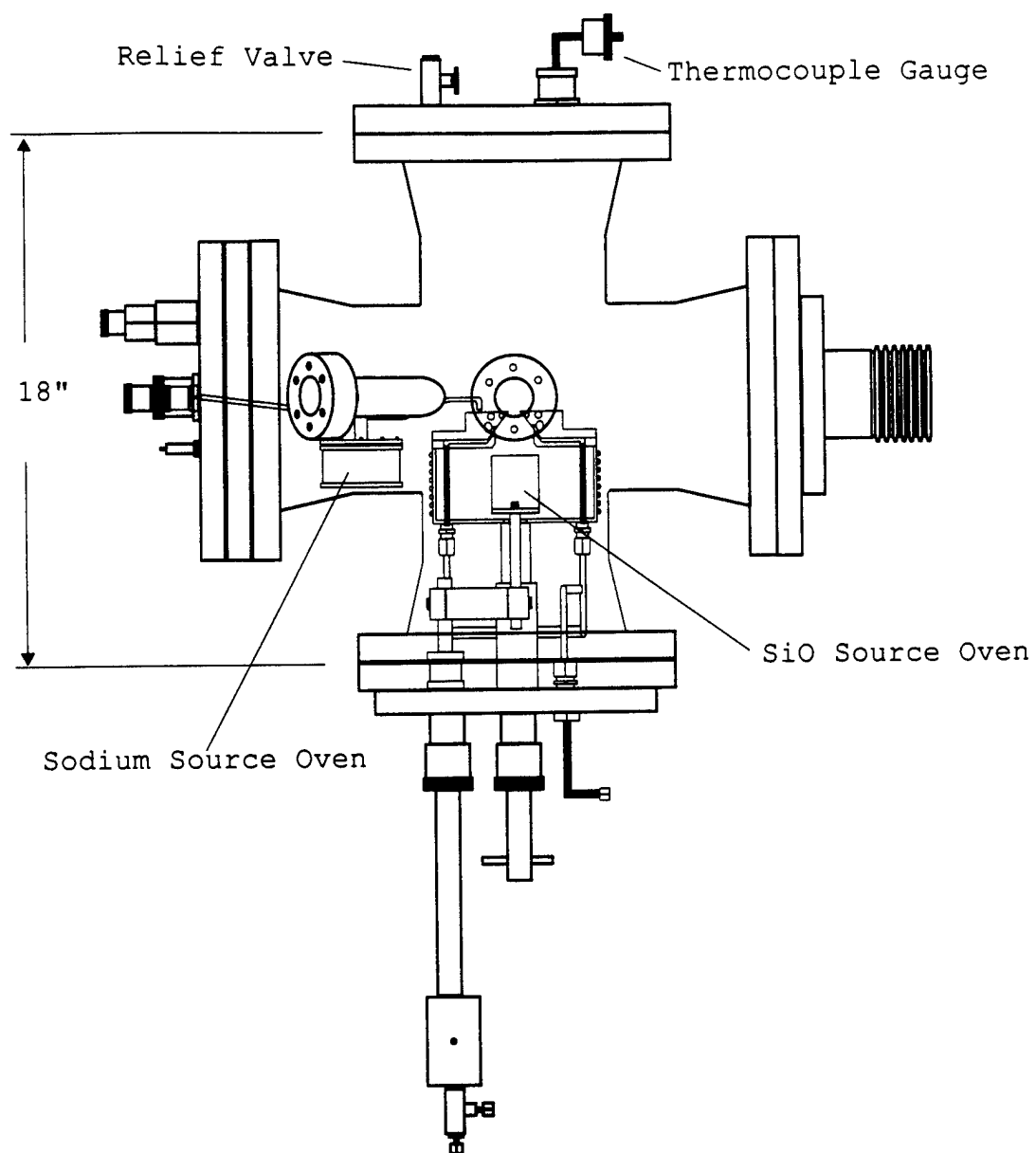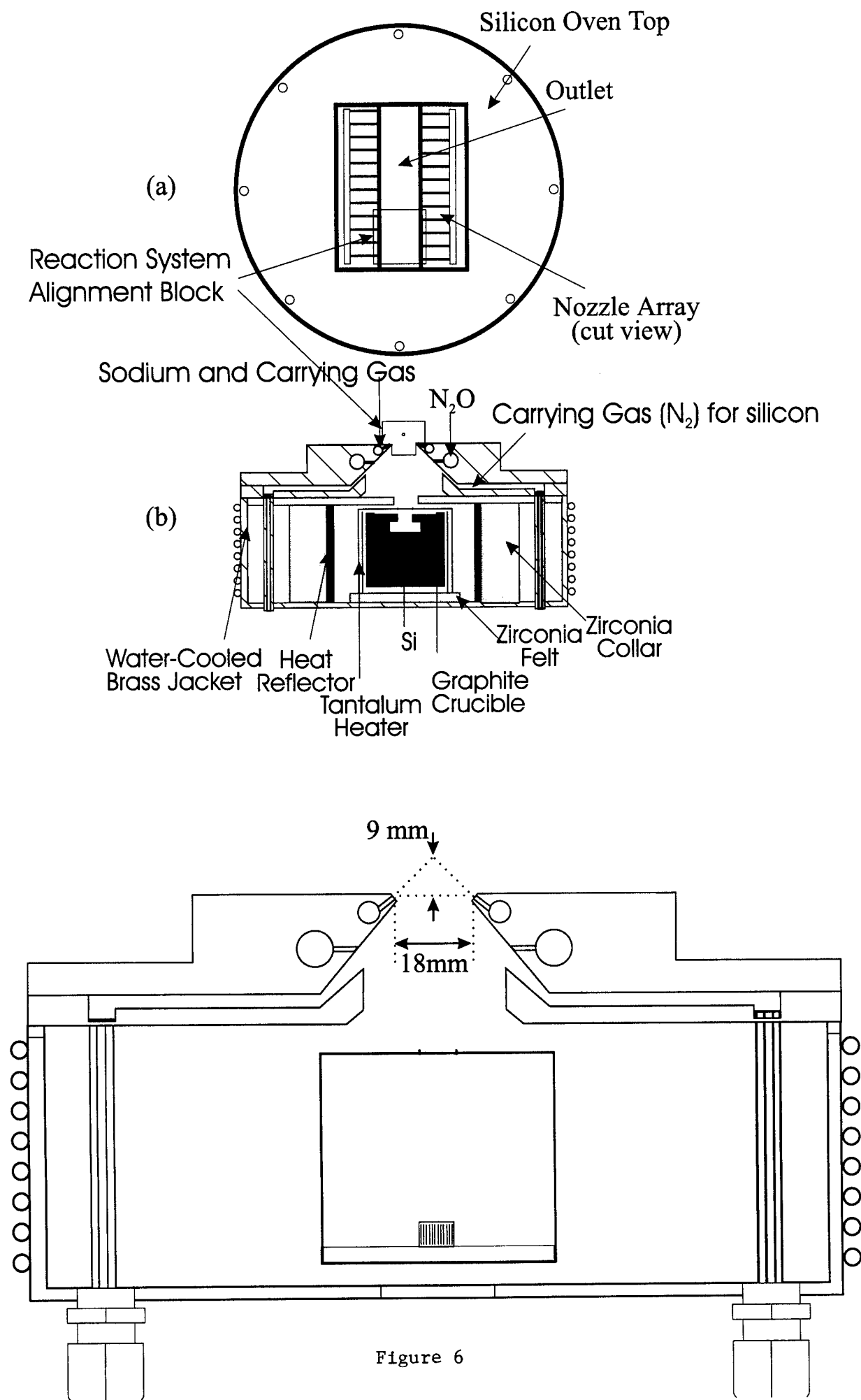Zirconia
Collar

9 mm

18mm

Figure 6

cleaning optical window configurations[7] as depicted in Figure 7(a) and (b). While no windows are inserted in the full cavity experiments, the gas flow (helium) through these devices does much to protect the mirrors in their vacuum mounts from any effluents associated with the reaction-energy transfer zone; however, the sensitive nature of the mirror surfaces, their extremely high reflectivity, and the inherently refractory and reactive nature of sodium vapor has made it also necessary to insert protective spray bars (helium) in front of the mirror stage assemblies. It is to be emphasized that the intrinsically low gain of the system we are employing suggests the need for high reflectivity mirror assemblies mounted in vacuum on remotely controlled translation stages, allowing creation of an optical cavity without window losses.

Schematics of the experimental configuration used to facilitate an SiO metastable-sodium atom interaction are depicted in Figures 5 and 6. The positioning of the associated vacuum chamber which contain sources to produce silicon and sodium vapors is depicted in Figure 4. The silicon source oven is indicated at the center of the chamber. A gain measurement or lasing experiment requires that the path traversing the self-cleaning optical window configuration[7] and the combined silicon-Na oven source configuration surrounded by the appropriate optical train be stringently aligned (Appendix A, gain; Appendix C, lasing demonstration). The required stability of the gas flows in the reaction-energy transfer zone is facilitated by a pumping stage which includes the incorporation of a large ballast tank between the reaction chamber and a Stokes model 212 vacuum pump.

Silicon monoxide was produced using the Si-N_2O reaction [Eqn. (1)]. Gas phase silicon was evaporated from an extended path length resistively heated oven consisting of a specifically designed carbon crucible surrounded by a tantalum jacket (Figs. 5,6). The efficiency of the
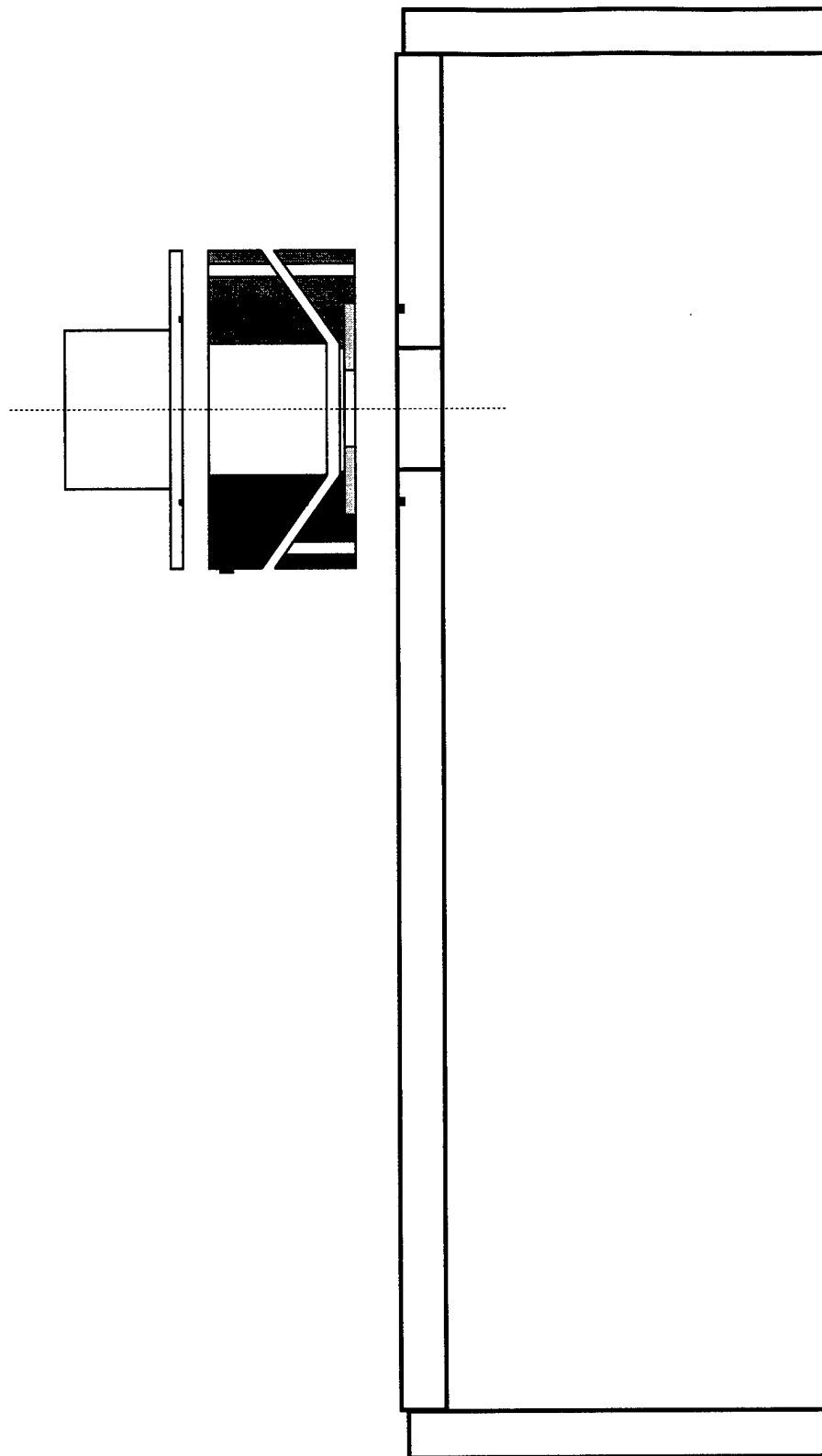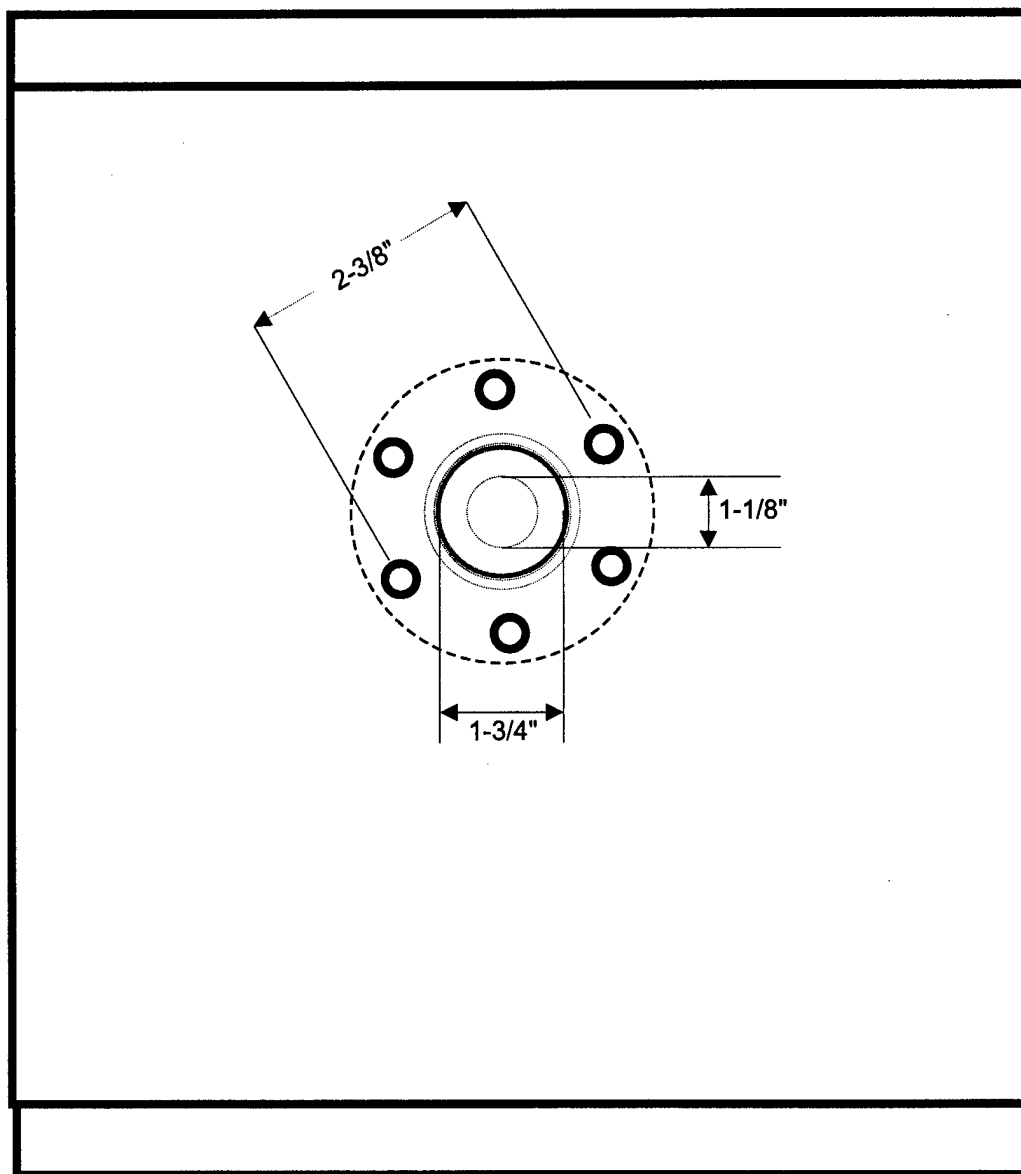
Figure 7a

2-3/8"

1-1/8"

1-3/4"

Figure 7b

tantalum heating element has been considerably improved from previous designs through small but significant modifications in its construction improving (1) electrical conduction through the element to enhance heating uniformity and (2) minimization of heat loss both from the tantalum radiator and carbon crucible through judicious incorporation of further insulation. The tantalum heating element is electrically isolated from the crucible using several layers of zirconia felt cloth which also provide insulation. Temperatures in the range of 1600° - 2000°C can be readily attained with this device, providing a high evaporative atomic concentration well in excess of 10^{14}/cc.

The silicon vapor exits the carbon crucible through a slit 3 mm wide by 5 cm in length. It is entrained in an N_2 carrying gas[1] (Appendix A) which also serves to focus the silicon flow. The N_2O oxidant is introduced through a concentric nozzle arrangement above the silicon oven (Figure 6 - cutaway view of silicon oven, supporting structure and surrounding water cooling jacket). The nozzle array depicted in Figure 6 provides for the concentric injection of sodium into the reaction zone. A sodium entrainment oven is positioned to the side of this assembly connected by stainless steel tubing (see also Fig. 5). This nozzle arrangement creates a Si-N_2O-Na reaction-energy transfer zone several centimeters (nominally 5 cm) long, affording a reasonable path length for gain and lasing studies.

The alignment of gain and lasing configurations is discussed in detail in Appendices A and C. In both experiments, alignment is set along an axis through the reaction-SiO-Na-energy transfer region (Figure 6) lying 9 mm above the top of the concentric oven-flow configuration. In order to approach a lasing demonstration an extensive procedure (Appendix C) involving (1) system alignment (He/Ne laser), (2) translation stage alignment, (3) reaction zone alignment, and

(4) laser mirror alignment is followed. Further alignment procedures are also instituted when using the fiber optic in conjunction with a spectrometer to monitor the wavelength dependence of the light emission from the Si/N$_2$O/SiO/Na reaction-energy transfer zone. In our laser demonstration experiments, we wish to create a cavity at the 9 mm point described above and downstream of this intersection point. This requires that the aligned mirrors and hence the cavity can be carefully and precisely translated vertically upward during an experimental run.

Before each experimental run, in the absence of vacuum, the optically aligned (Appendix C) mirrors are translated horizontally using the motor mic controllers. The translation of these mirrors must match precisely. Further, the angular movement (angular orientation) as a function of motor-mic control parameters of both the output coupling (mirror stage nearest power meter - Fig. 4) and feedback mirrors (for stage nearest fiber optic and spectrometer) has been periodically evaluated. The power meter signal level with an aligned output coupling mirror in place (feedback mirror removed) has been carefully checked to determine that the signal level due to the extended emission flame region (Fig. 6) is between 1.6 and 2.2 milliwatts. All mirrors used in the experiment have been checked with a green He/Ne laser and found to be between 0.02 and 0.03% transmissive as specified by the manufacturer. Several full cavity experiments have suggested important small modifications to the system and have clearly indicated the difficulty of cavity operation with high temperature refractory sources. For the next several months, we will continue to attempt to obtain lasing action from this system. However, it will be important for future considerations to seek alternate sources of the SiO metastables (silane based system[8]).

Participating Scientific Personnel

James M. Stephens, graduate student, currently Schlumberger Incorporated, Ph.D. thesis final revision expected by December 1999.

John Stout, graduate student.

Sarah Paukstis, graduate student.

Richard Lepkowicz, undergraduate student, currently graduate student at CREOL, University of Central Florida.

Professor Lee H. Sentman, Department of Aeronautical and Astronautical Engineering, University of Illinois, Urbana.

Professor James L. Gole, School of Physics, Georgia Institute of Technology, Atlanta, Georgia, principal investigator.

References

1. (a) G. J. Green and J. L. Gole, Chem. Phys. 100, 133 (1985) and references therein;

    (b) G. Hager, R. Harris, and S. G. Hadley, J. Chem. Phys. 63, 2810 (1975); G. Hager,

    L. E. Wilson, and S. G. Hadley, Chem. Phys. Letts. 27, 439 (1974).

2. See, for example, K. K. Shen, H. Wang, D. Grantier, and J. L. Gole, "Visible Chemical

    Lasers from Alkali Based Electronic Inversions", in Intense Laser Beams and

    Applications, SPIE Proceedings, Volume 1871, pg. 18 (1993), W. D. McDermott, Editor;

    J. R. Woodward, S. H. Cobb, K. K. Shen, and J. L. Gole, IEEE J. Quantum Electron. 26,

    1574 (1990).

3. A. Gaupp, P. Kuske, and H. J. Andra, Phys. Rev. A, Vol. 26, pp. 3351-3359 (1982).

4. S. A. Kandela, Appl. Optics, Vol. 23, p. 2151 (1984). X. He, B. Li, A. Chen, and C.

    Zhang, J. Phys. B, At. Molec. and Opt. Phys., Vol. 23, p. 661 (1990).

5. K. K. Shen, H. Wang, and J. L. Gole, IEEE J. Quantum Electron. 29, 2346 (1993).

6. (a) See for example, J. M. Stephens, J. L. Gole, L. H. Sentman, and M. Zaczek, "Potential

    for a Chemically Pumped Sodium Laser", AIAA-97-2425, AIAA 28th Plasmadynamics and

    Lasers Conference, June 23-25 (1997), Atlanta, GA. (b) A. E. Siegman, Lasers,

    University Science Books, Mill Valley, California, 1986, pp. 289-290. (c) G. Roll and J.

    Mentel, J. Phys. D Appl. Phys. 22, 483-487 (1989).

7. W. H. Crumley and J. L. Gole, Rev. Sci. Instrum. 57, 1692 (1986).

8. J. M. Stephens and J. L. Gole, Chem. Phys. 206, 173-183 (1996).

Appendix A

Measurement of Low-Level Gain in a

Visible Chemical Laser Amplifier

Measurement of Low-Level Gain in a Visible Chemical Laser Amplifier

James M. Stephens, John Stout, Joseph Abraham
Martin Neumann, and James L. Gole

School of Physics
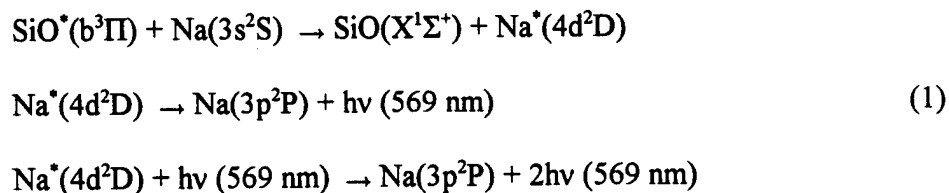Georgia Institute of Technology
Atlanta, Georgia 30332-0430

and

Lee H. Sentman

Aeronautical and Astronautical Engineering
University of Illinois
306 Talbot Laboratory
104 Wright St.
Urbana, IL 61801

I. Introduction

The development of a visible chemical laser, which requires the creation of a visible chemical laser amplifier and the demonstration of gain on transitions in the visible region of the spectrum, creates the need for careful zero power gain measurements. Here, we outline a procedure for high precision gain measurements which demonstrates that the sequence

$$SiO^*(b^3\Pi) + Na(3s^2S) \rightarrow SiO(X^1\Sigma^+) + Na^*(4d^2D)$$

$$Na^*(4d^2D) \rightarrow Na(3p^2P) + h\nu \ (569 \ nm) \tag{1}$$

$$Na^*(4d^2D) + h\nu \ (569 \ nm) \rightarrow Na(3p^2P) + 2h\nu \ (569 \ nm)$$

forms an energy transfer system which represents a viable chemical laser candidate based on amplification at 569 nm.[1]

To create a visible chemical laser amplifier, we make use of the metastable $b^3\Pi$ and a $^3\Sigma^+$ states of the SiO molecule which are formed in high quantum yield via the reaction

$$Si(^3P) + N_2O \rightarrow SiO^*(b^3\Pi, a^3\Sigma, A^1\Pi) + N_2 \quad . \tag{2}$$
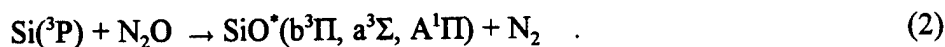
Here, the metastable triplet states which dominate the product formation process, are formed at an energy close to 3.5 eV and possess a lifetime of order 10 ms[1,2]. This suggests these metastables as potential donors for an energy transfer based visible laser amplifier resulting from the rapid pumping of select atomic transitions[3] isoergic with the metastables. Although potential molecular receptors have been suggested,[4] the multiplicity of states in a molecular species that are in near resonance with the donor metastables precludes an effective energy transfer to a limited number of levels. Given this consideration, the near resonant energy transfer pumping of atomic receptors is a more attractive means of producing electronic inversions.

The sodium atom represents one of the best candidates for energy transfer from

metastable SiO molecules. The $4d^2D$ level of sodium, which is not accessible via optical pumping from the ground electronic state, possesses several near resonances with the $SiO^*(b^3\Pi)$ state (Table I). Near resonant energy transfer pumping to this level, with subsequent decay and potential lasing, is illustrated in the Sequence (1) above. The relevant energy levels are outlined in Figure 1. In the Sequence (1) the $3p^2P$ level represents the terminal laser level which, as it decays rapidly to the $3s^2S$ ground state (the sodium D-line transition with $\tau_{rad} \sim 15$ ns),[5] facilitates the creation of an inversion. The decay from the $4d^2D$ level (with $\tau_{rad} \sim 80$ ns)[6] suggests the possibility for a high duty cycle. In fact, evidence for continuous amplification has been reported by Shen et al.[1,7] Using the Einstein A coefficients for the $4d^2D$ - $3p^2P$ transitions given in Table II, we can estimate a saturation intensity[8] of 6W-cm[-2] for a laser operating at 569 nm (at 500 K), which suggests that the SiO - Na* sequence represents a viable candidate for a visible chemical laser amplifier.

Here we outline a system for measuring gain on the Na $4d^2D$ - $3p^2P$ transition at 569 nm using a dual beam mode which allows compensation for fluctuations in the probe source output by comparing the beam which probes the gain medium with a reference beam, also from the probe source. In addition, both probe and reference beams are detected by a single photomultiplier tube in order to compensate for detector sensitivity fluctuations. These considerations define the gain measurement.

II. Gain Measurement System

The mechanical and optical layout for the zero power gain measurement are described in Figures 2 and 3. The optical system surrounds the SiO - Na* energy transfer pumping zone and

2

reaction chamber depicted in Figure 4 which has been described in detail elsewhere.[7,8] Here two 12" x 18" breadboards which flank the reaction chamber and a 4" x 36" connecting breadboard (Figure 2) are firmly mounted to the angle iron support structure for the vacuum-reaction chamber and the entire system is bolted to the floor of the laboratory.

The dual beam detection scheme used in these experiments is also depicted schematically in Figure 5. The employment of a dual beam spectro-radiometry system offers several advantages in a sensitive, stable measurement system. It provides correction for (1) source intensity fluctuations, (2) variations in source spectral density, (3) variations in detector spectral response, and (4) gain variations in detector and amplification stages. Further, for quantitative gain measurements, the stability of the probe signal sets a limit on the sensitivity of the measurement.

Following the optical path indicated in Figure 3, the output beam from the sodium discharge lamp passes through an iris diaphragm immediately adjacent to the lamp and then through a projection lens combination ℓ_1. It is necessary to maintain a nearly constant beam diameter through the SiO-Na* reaction energy transfer zone. This function is served by the lens systems ℓ_1 - ℓ_3. Lens ℓ_1, placed 35.5 cm from the discharge lamp, consists of two double convex lenses (38 mm and 333 mm focal length) held in contact to yield an effective focal length ~ 167 mm. The collimated beam passes from ℓ_1 to mirror m_1 and through beam splitter, b_1, where it is separated into the probe (through reaction-energy transfer zone) and reference beams. The probe (turned by m_2) and reference beams are routed through the mechanical chopper. A short parallel path for the two beams is requisite for their modulation by a single chopping wheel.

For the required phase sensitive studies, a 6/5 chopper wheel (Stanford Research Systems SR530) as outlined in Figure 5 was operated at a modulation frequency of 315 Hz, corresponding

3

to a frequency for the outer set of slots (f_{outer}) for the reference beam, and f_{inner} = 262.5 Hz for the inner set of slots corresponding to the probe beam.[9]

After modulation, the probe beam is made to traverse the experimental chamber employing mirrors m_3 and m_4, and passes through lens ℓ_2 positioned between the two mirrors. The reference beam, emanating from b_1, passes through lens ℓ_3. The lenses ℓ_2 and ℓ_3 are identical double convex lens combinations (38 and 250 mm focal length) which are placed 65 cm from ℓ_1 for both the probe and reference beams. While the probe beam traverses the reaction-energy transfer zone to a second beam splitter, b_2, the reference beam is steered to b_2 by the mirror, m_5. The probe beam passes directly through b_2 to the monochromator-detection system (1 meter Spex blazed at 500 nm) while the reference beam is reflected by b_2 to the monochromator. It is at b_2 that the probe and reference beams are combined, pass through a "pinhole" orifice to the entrance slit of the monochromator detection system, and are made to impinge in the same region on a single detector. By setting the iris diaphragm to 6 mm, the system produces a probe beam of ~ 1.2 cm diameter in the reaction-energy transfer zone.

The distinctly modulated probe and reference beams impinging on the single detector (Hamamatsu 1P28 photomultiplier at the monochromator exit port) are separated by phase sensitive detection. Two lock-in amplifiers (Stanford Research Systems SR510), one referenced to the probe beam waveform (probe lock-in) and the other to the reference beam waveform (reference lock-in) are used for the measurements.[9] *Gain determination requires that phase sensitive detection be employed to distinguish the probe beam from the spontaneous emission associated with the amplification medium.* With the dual lock-in system, the demodulated output from the reference lock-in serves as a *normalizing* input to the probe lock-in. Here, the

4

normalization function is performed by the probe lock-in.

Considerable effort was expended to insure equivalent paths for the probe and reference beams in the design of the optical system. This is required since compensation for source output variation demands that: (1) the reference signal possess the same temporal behavior as the probe and, (2) the probe and reference optical systems image the same portion of the source upon the detector.

If the probe and reference beam path lengths are maintained equal to within one centimeter, the traversal time of each beam will be equal to within several picoseconds. Within the parameters selected for the lock-in (time constant ~ 1 second) variations in the Na lamp output, comparable to the difference in arrival times of the probe and reference beams, will be insignificant. Further, as identical corresponding optical elements are placed in equivalent positions in their respective optical paths, the probe and reference systems are expected to image the same portion of the Na lamp source onto the detector. However, careful alignment and testing is necessary.

Current to voltage conversion of the Hamamatsu 1P28 output signal is accomplished with a National Semiconductor LM4250C operational amplifier. The lock-in detectors provide three outputs; the probe lock-in provides the demodulated probe signal and a normalized probe signal, the reference lock-in provides a demodulated reference signal. The normalized probe signal, which is defined as the probe signal divided by the reference signal, is obtained as the SR-510 normalizes the signal it measures by the reference signal, which it uses as input. These output voltages are subjected to analog to digital conversion (ADC) by a Real Time Devices ADA 2000 interface board and subsequently recorded by a personal computer.

5

III. Propagation and Gain Determination

In order to evaluate the detection equation for the system probe and reference beams,[10] it is necessary to evaluate the effect of the system components on the Na lamp beam radiance, L_o (watt-m^{-2}-sr^{-1} subtended from the lamp). We note that the probe beam passes through a window upon entering the reaction-energy-transfer zone. Immediately prior to entering the reaction zone, at position P_1 in Figure 3, the radiance of the probe beam, L_1, may be expressed as

$$L_1 = (t_{BP} t_1 t_2 r_b r_1 r_2 r_3 r_4 t_w) L_0 \cdots \qquad (3)$$

In this expression, t_{BP} is the transmittivity of the bandpass filter, r_b is the reflectivity of the beamsplitter, $r_{1,2,3,4}$ are the reflectivities of the mirrors indicated by the subscripts, t_1 is the transmittivity of lens ℓ_1, t_2 of lens ℓ_2, and t_w is the window transmittivity.

The radiance upon exiting the reaction zone, at position P_2, is then,

$$L_2 = e^{\alpha \ell} L_1 \cdots \qquad (4)$$

where the quantity α is the small signal gain coefficient and ℓ is the effective gain length. The amplification ratio A_R is

$$A_R = \frac{L_2}{L_1} = e^{\alpha \ell} \cdots \qquad (5)$$

and the small signal gain coefficient is calculated from the amplification ratio as

$$\alpha = \left(\frac{1}{l} \right) \ln (A_R) \cdots \qquad (6)$$

6

The radiance of the probe beam at the detector

$$L_{probe} = t_w t_b t_{mono} L_2 \cdots \tag{7}$$

where the transmittivities of the beamsplitter (b_2) and of the monochromator have been expressed as t_b and t_{mono}. Thus, the radiance at the detector is related to the initial radiance by

$$L_{probe} = \left\{ t_w^2 t_{BP} t_b r_b r_1 r_2 r_3 r_4 t_1 t_2 t_{mono} e^{\alpha \ell} \right\} L_0 \cdots \tag{8a}$$

$$= \tau_{probe} L_0 \cdots \tag{8b}$$

where τ_{probe} is the propagance of the probe beam path.[11]

In analogy, the radiance of the reference beam at the detector is given by

$$L_{ref} = \left\{ t_{BP} t_b r_b r_1 r_5 t_1 t_3 t_{mono} \right\} L_0 \cdots \tag{9a}$$

$$= \tau_{ref} L_0 \cdots \tag{9b}$$

where τ_{ref} is the propagance for the reference beam, a constant, and L_0 is the radiance from the lamp.

The radiant fluxes at the detector due to the probe and reference beams are respectively

$$\Phi_{probe} = L_{probe} G_{probe} \cdots \tag{10a}$$

$$\Phi_{ref} = G_{ref} L_{ref} \cdots \tag{10b}$$

7

where $G_{probe} = G_{ref}$ corresponds to the geometric extent calculated as the area of the monochromator input aperature multiplied by the solid angle subtended by the radiation incident on this aperture.

The output electrical signals can be expressed as

$$S_{probe} = G_{probe} R_{probe} \tau_{probe} L_0 \cdots \qquad (11a)$$

$$S_{ref} = G_{ref} R_{ref} \tau_{ref} L_0 \cdots \qquad (11b)$$

where S_{probe} and S_{ref} are the probe and reference signals and R_{probe} and R_{ref} are the responsivities accounting for the conversion of the optical signal to an electrical signal. The responsivity can include the response of the photomultiplier to the incident radiation (the product of the photocathode radiant sensitivity and PMT current gain), the amplification due to any preamplification stages between the PMT and the lock-in amplifier, and the responsivity of the device reading the PMT output, in this work the lock-in amplifier. The final signal, S_{probe}, will be a voltage, the demodulated output of a lock-in amplifier. Note that equations (3) - (11) do not include the temporal behavior of the devices present in the system.

IV. Compensation for Source and Detector Fluctuations

For the dual beam measurements of this study, the normalized signal,

$$S_{norm} = \left(\frac{S_{probe}}{S_{ref}} \right) \cdot V_F^{ratio} \cdots \qquad (12)$$

a voltage, is proportional to the ratio of the probe and reference signals, scaled to the full scale output, V_F^{ratio}, of the phase sensitive detector. Thus the normalized signal can be expressed as

$$S_{norm} = \frac{G_{probe}R_{probe}\tau_{probe}L_0}{G_{ref}R_{ref}\tau_{ref}L_0} \cdot V_F^{ratio} = \frac{R_{probe}\tau_{probe}}{R_{ref}\tau_{ref}} \cdot V_F^{ratio} \cdots \tag{13}$$

where we have noted that the normalized signal is independent of the effects of source fluctuation. The steady-state responsivity for the combination of photomultiplier (PMT), current to voltage conversion circuit, and lock-in amplifiers can be evaluated to obtain the complete detection equations[12-15] for a single detector (after analysis of the lock-ins)

$$S_{probe} = L_0\tau_{probe}GB_vA_cR_F\,[(\pi/4\sqrt{2}) \cdot (V_F/S_D)_{probe}] \cdots \tag{14a}$$

$$S_{ref} = L_0\tau_{ref}GB_vA_cR_F\,[(\pi/4\sqrt{2}) \cdot (V_F/S_D)_{ref}] \cdots \tag{14b}$$

where B_v is the sensitivity of the PMT photo-cathode, A_c is the current gain, R_F is the operational amplifier feedback resistance, V_F the lock-in full scale output voltage, and S_D is the full scale sensitivity. The normalized signal, the ultimate limits of whose stability is determined entirely by the stability of the lock-in amplifier outputs, is then

$$V_{norm} = \left(\frac{\tau_{probe}(V_F/S_D)_{probe}}{\tau_{ref}(V_F/S_D)_{ref}}\right) \cdot V_F^{ratio} \cdots \tag{15}$$

The low-pass filtering operation which the lock-ins perform introduces a time constant to our

9

evaluation as the lock-in response corresponds to a convolution of the impulse response of the low pass filter with the product of the modulated signal and reference waveforms. The demodulated output, $V_0(t)$, is then

$$V_0(t) = [V_S(t) \cdot f_{mod}(t) \cdot f_{reference}(t)] \otimes h_L(t) \dots \tag{17}$$

where $V_S(t)$ is the signal, $f_{mod}(t)$ and $f_{reference}(t)$ are respectively the modulation and reference waveforms, and $h_L(t)$ the low-pass filter impulse response.[14,16] The normalization of the probe to the reference signal thus requires that the impulse response functions for the two lockins (Figure 5) should be matched as closely as possible usually by choosing identical time constants.[a]

V. Estimates of Optical Flux Transmission

A collimation is introduced by the lens systems ℓ_1 and ℓ_2 in order that a beam of uniform diameter and flux density pass through the reaction zone. The luminescence of the OSRAM sodium discharge lamp (Figure 2) can be calculated to be 41 lm-cm^{-2} - sr.[17] To obtain the radiance at 569 nm, we assume that most of the output is radiated in the sodium D-lines and scale the 569 nm radiance to one of the components of the D-line.

The luminance is obtained from the known radiance distribution

$$L_v = 683 \sum_{all\ lines} \int_{line} L_\lambda(\lambda) \cdot V(\lambda) \cdot d\lambda \dots \tag{18}$$

---

[a]If two different lock-in models are used, the matching process is more complex.

10

where $L_\lambda(\lambda)$ is the spectral radiance, $V(\lambda)$ is the photopic response, and 683 is the standard photometric-radiometric conversion factor. Taking the photopic response as approximately constant for a given atomic feature, we have

$$\int_{line} L_\lambda(\lambda) \cdot V(\lambda)\, d\lambda \cong V(\lambda_0) \int_{line} L_\lambda(\lambda) \cdot d\lambda \ldots \tag{19a}$$

$$\cong V(\lambda_0) \cdot \delta\lambda \cdot L_\lambda(\lambda_0) \ldots \tag{19b}$$

$$= V(\lambda_0) \cdot L_{line} \ldots \tag{19c}$$

Assuming that the vast majority of the Na lamp energy is radiated into the Na D-lines and that the photopic response is virtually identical for the D_2 and D_1 components at 589 and 589.6 nm,

$$L_v \cong 683 \cdot V(D\text{-}lines) \cdot [L_{D_1} + L_{D_2}] \ldots \tag{20}$$

Scaling to one of the D-line components gives

$$L_v \cong 683 \cdot V(D\text{-}lines) \cdot [1 + L_{D_1}/L_{D_2}] \cdot L_{D_2} \ldots \tag{21a}$$

11

$$= 683 \cdot V(D\text{-}lines) \cdot [1 + L_{photo}^{D_1}/L_{photo}^{D_2}] \cdot L_{D_2} \cdots \qquad (21b)$$

where the ratio of the radiances is taken equal to the ratio of the photo currents, I_{photo}, determined for each D-line component from a representative scan of the lamp output. Appropriate photocurrent values for the D-line components and the 568.2 nm and 568.9 nm lines are taken from a spectral scan of the discharge lamp. These photocurrents, photopic response values,[b] monochromator transmissivities, and PMT photocathode radiant sensitivities are given in Table III. Monochromator transmissivities were obtained from $t_{mono} = r^2 P_{disp.}$ where $r = 0.88$ is the reflectivity of the Czerny-Turner spectrometer mirrors,[11,17] and P_{disp} is the diffracted power.[18]

The radiance at the D_2 line is estimated as

$$L_{D_2} \cong \frac{L_v}{683 \cdot V(D\text{-}line) \cdot [1 + I_{photo}^{D_1}/I_{photo}^{D_2}]}$$

$$L_{D_2} \cong \frac{41\, lm \cdot cm^{-2} \cdot Sr^{-1}}{683\, lm \cdot W^{-1} \cdot 0.768 \cdot [1 + 137/112]}$$

$$L_{D_2} \cong 3.5 \times 10^{-2}\, W \cdot cm^{-2} \cdot sr^{-1}$$

The ratio of the radiances at 569nm and for the Na-D_2 line are determined as

$$\frac{L_{569nm}}{L_{D_2}} = \frac{t_{mono}^{D_2} \cdot S_{D_2}}{t_{mono}^{569nm} \cdot S_{569nm}} \cdot \frac{I_{photo}^{569nm}}{I_{photo}^{D_2}} \cdots$$

and

---

[b]Interpolated from the Oriel Corporation Catalog.[17]

$$L_{569nm} \cong \frac{0.48 \cdot 6.7\,(mA/W)}{0.50 \cdot 9.5\,(mA/W)} \cdot \frac{1.0 x\,10^{-7} A}{1.37\,x\,10^{-5} A} \cdot 3.5\,x\,10^{-2}\,W \cdot cm^{-2} \cdot sr^{-1} \cong 1.7\,x\,10^{-4}\,Wcm^{-2} \cdot sr^{-1}$$

The irradiance in the reaction-energy transfer zone is obtained from the product of the radiance, the appropriate solid angle, and the propagance at the position of interest. The solid angle subtended by the radiation coupled from the Na-lamp into the optical system, defined by the aperture stop at lens, ℓ_1 (1.2 cm), and the lamp-lens distance (35.6 cm) is

$$\Omega_0 \cong \pi \cdot (0.6\,cm)^2/(35.6\,cm)^2 = 9 \cdot 10^{-4}\,sr$$

Assuming that the lamp output is restricted to a 6 mm diameter (iris diaphragm), the geometric extent (Figure 6) is

$$G_0 = \pi \cdot (0.3\,cm)^2 \cdot 9\,x\,10^{-4}\,sr \cong 2.5\,x\,10^{-4}\,cm^2 \cdot sr$$

The propagance of the optical beam path from the lamp to the reaction-energy transfer zone is

$$\tau = (0.92)^4 \cdot (0.5) \cdot (0.88)^4 \cong 0.21$$

where the beam has passed through a 50/50 beam splitter, suffered reflections from four mirrors ($r = 0.88$), and transmitted through three lens elements ($\ell_1(2)$, ℓ_2) and a window (0.92). The flux in the reaction chamber is thus

$$\Phi_1 = r \cdot G \cdot L_0$$
$$\approx (0.21) \cdot (2.5 \times 10^{-4} \, cm^2 \cdot sr) \cdot (1.8 \times 10^{-4} \, W \cdot cm^{-2} \cdot sr^{-1})$$
$$\cong 9.5 \times 10^{-9} \, W$$

which, for a 1 cm diameter beam in the reaction zone, corresponds to an irradiance

$$E = \Phi_1 / area \approx 9.5 \times 10^{-9} \, W/\pi \cdot (0.5 \, cm)^2 \cong 1.2 \times 10^{-8} \, W \cdot cm^{-2}$$

With this value of the irradiance, it is clear that the Na-lamp used in these experiments will not saturate the transitions of interest (Figure 1) in the reaction-energy-transfer zone.

Similar considerations allow an estimate of the signal expected at the detector due to the lamp source. Relevant quantities are outlined in Table IV (see also Figure 6(b)). With a monochromator transmissivity of 0.5, two beam splitters (0.5), four steering mirrors, m_1 - m_4 (0.88), three lens elements, and two windows (0.92), the propagance is

$$t \cong (0.92)^5 \cdot (0.5)^3 \cdot (0.88)^4 \cong 0.05$$

and the radiance is

$$L_{probe} = \tau \cdot L_0 \cong (0.05) \cdot (1.7 \times 10^{-4} \, W \cdot cm^{-2} \cdot sr^{-1})$$
$$= 8.5 \times 10^{-6} \, W \cdot cm^{-2} \cdot sr^{-1}$$

The remaining relevant quantities are given in Table 5 where the geometric extent, G_F, is the product of the monochromator slit area, A_{mono}, and the solid angle subtended by the incident radiation at the entrance slit.

14

VI. Evaluation of System Detection Sensitivity and Signal Detection Limits

Detection Sensitivity

In order to evaluate the detection system sensitivity it is necessary that one evaluate (1) the performance of the optical components in the detection system and (2) the noise characteristics of the PMT and the associated instrumentation as outlined in Figure 5. We have tested the limits of the detection system sensitivity using the tightly controlled rotational adjustment of a polarizing filter to probe a continuous variation (with rotation angle) in the attenuation of the probe beam (Figures 2,3). In implementing this test, one must be cognizant that the attenuation produced is also dependent on the polarization state of the beam and determined also by the polarizing properties of the optical elements. Thus, the information necessary to evaluate the sensitivity was obtained by evaluating the polarization dependence of the transmissivity of the probe beam through the combination of the two beam splitters, b_1 and b_2, (depicted in Figures 2 and 3) and a rotating polarizer.

Exploiting the polarization properties of the beam splitters makes it possible to devise a suitable test of sensitivity using only one rotating polarizer filter placed in the probe beam. Indeed, the polarization of the systems optical components are carefully considered as we account for the action of the polarizer. In Appendix A, we consider the derivation of the transmittivity through the two polarizing beam splitters and a rotating polarizer placed between them to arrive at the appropriate means for evaluating the ratio of the probe beam signals as a function of small changes in the polarization filter angle. We have used this approach, which is also useful as a general method to test a gain/absorption measurement system, as a means of evaluating the accuracy with which the amplification ratio, A_R (Eq. (5)), could be determined. The data given in

15

Appendix A demonstrates that the change in signal, predicted to result as the polarizer is rotated, *corresponds to the feasible measurement of a gain coefficient less than one part per thousand* (10^{-3}).

As we record the three data channels corresponding to the probe, reference, and normalized DC output from the lock-in amplifiers, a comparison can be made between single channel and normalized data acquisition. *We find that the normalized signal has an uncertainty notably less than a part per thousand (10^{-4} range).* This suggests that an amplification of the probe beam of approximately one part per thousand should be readily detectable through observation of the normalized signal. Further, the advantage of normalization becomes more evident when the system is less well behaved. Thus, in this study, a gain determination involves the comparison (amplification ratio) of two series of normalized data points; one in which the gain condition is absent and one in which the gain condition is present. The performance of the detection system also depends critically upon careful optical alignment.

By normalizing the probe (or reference) signal to itself, it is possible to test the limits of the electronics used in the experiment. This is made possible by tuning both lock-in detectors to the same modulation frequency so that they both detect the signal produced by the same beam. The reference lock-in then provides a normalization signal to the probe lock-in that is identical to the signal detected by the probe lock-in. Any variation in the normalized output is then due to the limitations of the lock-in detectors. It is easily demonstrated that the normalized output is stable to the parts per thousand range when this test is performed, even when there is obvious drift in the probe and reference channels.

16

Signal Detection Limits

The noise characteristics of the photomultiplier tube (PMT) and associated instruments indicated in Figure 4 also establish a limit on the smallest amplification that can be detected. The probe power determined from the measured photocurrent (Table IV) expressed as a flux is

$$\Phi = I_{photo}^{569nm}/B_v A_c = 9.74 \; x \; 10^{-8} A / 6.54 \; x \; 10^5 \cdot 9.5 \; x \; 10^{-3} A \cdot W^{-1} \approx 1.6 \; x \; 10^{-11} \; W \; . \qquad (22)$$

This power, when compared to the smallest signal the PMT can detect provides an estimate for the detection limit of the amplification set by the PMT. Using an expression for the minimum detectable power given by Yariv[12]

$$P_{min} = (hc/\eta\lambda) \cdot \sqrt{(I_s \cdot \Delta f/e)} \; ... \qquad (23)$$

where I_s is the photocathode signal current, η is the quantum efficiency (ratio of photoelectrons emitted at the cathode per incident photon estimated as 1:50 from the Hamamatsu PMT handbook[19]) and Δf is the bandwidth determined by the lock-in time constant.

The photocathode signal, I_s, can be estimated from Table IV to be $1.5 \; x \; 10^{-13}$ A ($9.74 \; x \; 10^{-8}/6.54 \; x \; 10^5$). The minimum detectable change is conservatively estimated as $1.7 \; x \; 10^{-14}$ W assuming that the bandwidth, Δf, is one Hz, a conservatively high value based on the time constants for the lock-ins used in this study.[20]

The change in PMT output resulting from the minimum detectable change in power is obtained by substitution of the minimum detectable (change in) power into Equation 22 yielding

17

$$I_{photo} = \Phi B_v A_c = (1.7 \, x \, 10^{-14} W) \cdot (9.5 \, x \, 10^{-3} A \cdot W^{-1}) \cdot (6.54 \, x \, 0^5) \cong 1.1 \, x \, 10^{-10} A$$

which is comparable to the shot noise.

The shot noise, again for a 1 Hz bandwidth, can be estimated[20] to be 1.4 x 10^{-10} A, almost three orders of magnitude greater than the thermal noise current which can be determined to be ~ 4 x 10^{-13} A. The PMT shot noise is the dominant noise source, indicating that feedback resistance does not appreciably degrade the signals being supplied to the lock-in detectors. The estimated magnitude of the shot noise (1.1 x 10^{-10} A) is approximately one part per thousand of the probe signal strength (9.74 x 10^{-8} A).

Again assuming a 1 Hz bandwidth, the noise current introduced by the LM 4250C operational amplifier is negligible. The minimum change observable in a signal imposed by the lock-in amplifiers is substantially smaller than that imposed by the photomultiplier, and the quantizing error introduced by the resolution of the lock-in analog outputs and subsequent analog to digital conversion (ADC) is also negligible.

The analog to digital conversion is accomplished by a Real Time Devices ADA 2000 12-bit interface board. This device performs a staircase type ADC operation: the ten-volt analog input range corresponds to 2048 steps. This, in turn, corresponds to a resolution of approximately five parts per ten thousand. It appears that the detection limit is, in principle, determined by the limits of the PMT. If the PMT is operated at moderate voltage, amplifications approaching values as small as a part per thousand may be expected to be detectable disregarding noise or other unforseen effects that may degrade the detection system's performance.

VII. The Evaluation of Gain

A more detailed schematic of the silicon source configuration used to facilitate the SiO - Na energy transfer process including the entrainment gas, oxidant, and Na nozzle arrays is depicted in Figure 7. This device is discussed in detail elsewhere[7,8,20] and will be only briefly outlined. Here, the emphasis is on defining the probe beam region, corresponding to the Na nozzle array intersection point, very close to 9 mm above the top of the nozzle array. In all of the experimental gain measurements conducted in this study, a detailed alignment procedure was followed to insure that the probe beam (Figures 2,3) passed through the line created by the series of intersection points of the nozzle arrays. Further, for this experiment, the required stability of the gas flows in the reaction-energy transfer zone is facilitated by the incorporation of a large ballast tank between the reaction chamber and the Stokes model 212 vacuum pump.

Silicon monoxide was produced using the Si-N_2O reaction [Eqn. (1)]. Gas phase silicon was evaporated from an extended path length resistively heated oven consisting of a carbon crucible surrounded by a tantalum jacket (Fig. 7[20]). The tantalum heating element is electrically isolated from the crucible using a layer of zirconia cloth.[7,22] Temperatures in the range of 1600° - 1800° C can be attained with this device, providing a high evaporative atomic concentration which can be in excess of 10^{14}/cc.

The silicon vapor exits the carbon crucible through a slit 3 mm wide by 5 cm in length. The oxidant is introduced through a concentric nozzle arrangement above the silicon oven. A cutaway view of the silicon oven, supporting structure and surrounding water cooling jacket is illustrated in Fig. 7. The nozzle depicted in this figure provides for concentric injection of sodium into the reaction zone. The sodium entrainment oven is positioned to the side of this assembly

19

connected by stainless steel tubing (see also Fig. 4). This nozzle arrangement creates a Si-N$_2$O-Na reaction-energy transfer zone several centimeters (nominally 5 cm) long, affording a reasonable path length for the gain studies.

After testing and experimentation with the detection system as outlined in Section VI, an extensive series of gain measurement was undertaken. The temperature range over which the silicon oven systems were operated (brought to temperatures exceeding the melting point (1680 K)) correlate with evaporation rates[20,21] in the range from 4 x 10^{-5} (1900 K) to 5 x 10^{-4} (2100 K) gram-cm^{-2} sec^{-1} corresponding to fluxes ranging from 9 x 10^{17} to 1 x 10^{19} cm^2-sec^{-1}. At the operating conditions of the experiments, the sodium temperature was ~ 600°C (correlates with a lower oven container current of 5 amps and an upper nozzle compartment current of 6 amps, column 5 of Table V) corresponding to a vapor pressure of one Torr.[22]

The following data collection procedure was adopted: Two hundred data points were collected to produce an amplification ratio. For the first 100 data points, no oxidant flow was present. The oxidant flow was then activated for the collection of the next 100 data points. The oxidant flow was again stopped, and the cycle was repeated. The last 75 data points of each 100 point half cycle were averaged to produce the signal value for the given half cycle. The signal levels recorded in the oxidant-on and oxidant-off configurations were then compared. The ratio of these two values produces the amplification ratio (AR)

$$A_R = \frac{[S_{probe}]_{oxidant\ on}}{[S_{probe}]_{oxidant\ off}}$$

20

from which the zero power gain coefficient is calculated (Equation 6).

Only the last 75 data points from each half cycle, rather than the full 100 points, are averaged to allow for system and lock-in amplifier response. To collect 25 data points requires approximately 5 seconds. Discarding the first 25 data points after the oxidant flow is switched on or off, then, allows the system to settle to within ten percent of its steady state response level.

Data taken for several gain determinations are summarized in Table V. In all cases, the results of data analysis for the normalized data acquisition channel are presented. For runs 3-6, however, increased data acquisition capability allowed the simultaneous acquisition of data for normalized, probe, and reference channels.[20] As test scans are recorded when the sodium and silicon oven sources are brought to temperature, the normalized signal level is found to decrease as the silicon oven approaches its operating temperature. When all three channels are recorded, it is observed that the probe signal decreases with increasing silicon oven temperature. The normalized signal is observed to decrease as a result. While the dual beam technique cannot compensate for the temperature dependence of the propagance of the probe beam, for gain measurements at a given temperature, the drift in the probe and reference beams is negligible. Therefore, if the temperature is reasonably steady during a data collection run, the compensation technique will readily account for lamp or detector variation as intended. Thermal lensing effects do not appear to prejudice the data presented in Table V.

The results presented in Table V suggest a gain coefficient conservatively estimated as 0.8 - 1.5 x 10^{-3} cm^{-1}, deduced as the probe beam traverses the specific aligned path indicated in Figure 7. A limited range of carrier gas and reactant parameter space has been evaluated with these measurements. The ideal and much more complex experiment would involve the

simultaneous scanning of the flow field to determine the maximum gain region as a function of oxidant flow, silicon and sodium oven temperatures, and carrier gas flows.

In the outlined experiments, the oxidant flow was adjusted to maximize, to the greatest extent possible, the 569 nm transition. However, oxidant flow rates were found which, if exceeded, produced an apparent decrease of the 569 nm emission in the region of the probe beam. While the precise source of this decrease was not identified, it most likely results from the modification of the location of the zone of optimal gain due to the adjustment in the reactant flows. In the experiments summarized here, every attempt was made to adjust the gain volume distribution so as to maximize the gain across the probe beam region. Once this maximum value was approached, the N_2 carrier gas flow rates were adjusted to reduce the intensity of the D-line with respect to the 569 nm line.[1,7] The optimum oxidant flow rates are found to be correlated with very high silicon oven temperatures. Indeed, as Table V would suggest, the optimization of the silicon atom flux is most crucial to the observation of a gain condition. The efficient and optimized generation of SiO metastables is key to the attainment of the gain condition in this system.

References

1. See, for example, K. K. Shen, H. Wang, D. Grantier, and J. L. Gole, "Visible Chemical Lasers from Alkali Based Electronic Inversions", in Intense Laser Beams and Applications, SPIE Proceedings, Volume 1871, pg. 18 (1993), W. D. McDermott, Editor; J. R. Woodward, S. H. Cobb, K. K. Shen, and J. L. Gole, IEEE J. Quantum Electron. 26, 1574 (1990).

2. G. J. Green and J. L. Gole, Chem. Phys. 100, 133 (1985) and references therein; G. Hager, R. Harris, and S. G. Hadley, J. Chem. Phys. 63, 2810 (1975); G. Hager, L. E. Wilson, and

   S. G. Hadley, Chem. Phys. Letts. 27, 439 (1974).

3. J. L. Gole, K. K. Shen, H. Wang, C. B. Winstead, and J. Stephens, "Chemically Driven Visible Laser Amplifiers and Oscillators Based on Fast Electronic Energy Transfer", AIAA 93-3209, AIAA 24th Plasmadynamics and Lasers Conference, July 6-9, 1993, Orlando, FL.

4. N. G. Basov, V. F. Gavrikov, S. A. Pozdneez, and V. A. Shcheglov, Sov. J. Quantum Electron. 17, 9, 1987.

5. A. Gaupp, P. Kuske, and H. J. Andra, Phys. Rev. A, Vol. 26, pp. 3351-3359 (1982).

6. S. A. Kandela, Appl. Optics, Vol. 23, p. 2151 (1984). X. He, B. Li, A. Chen, and C. Zhang, J. Phys. B, At. Molec. and Opt. Phys., Vol. 23, p. 661 (1990).

7. K. K. Shen, H. Wang, and J. L. Gole, IEEE J. Quantum Electron. 29, 2346 (1993).

8. (a) See for example, J. M. Stephens, J. L. Gole, L. H. Sentman, and M. Zaczek, "Potential for a Chemically Pumped Sodium Laser", AIAA-97-2425, AIAA 28th Plasmadynamics and

23

Lasers Conference, June 23-25, (1997), Atlanta, GA. (b) A. E. Siegman, Lasers, University Science Books, Mill Valley, California, 1986, pp. 289-290. (c) G. Roll and J. Mentel, J. Phys. D Appl. Phys. 22, 483-487 (1989).

9. (a) LIA note 22, "Lock-In Applications Anthology", D. Malchow, ed., (c) 1986, EG&G Princeton Applied Research. (b) M. L. Mead, "Lock-In Amplifiers: Principles and Applications", (c) 1983: Peter Perigrinus, Ltd., 208-210; LIA note 51, "Lock-In Applications Anthology", D. Malchow, ed., (c) 1986, EG&G Princeton Applied Research.

10. F. E. Nicodemus, "Self-Study Manual on Optical Radiation Measurements: Part I-Concepts", Chapters 4 and 5, NBS Tech Note 910-01, U. S. Government Printing Office, 1978.

11. (a) F. Hengsterber, "Absolute Radiometry", Academic Press, 1989, pg. 14. (b) R. W. McCluney, "Introduction to Radiometry and Photometry", Artech House, Inc., 1994.

12. A. Yariv, Optical Electronics, Third Ed., Holt, Rinehart, and Winston, Inc., 1985.

13. A. J. Diefenderfer, "Principles of Electronic Instrumentation", W. B. Saunders Company, 1979, p. 392.

14. M. L. Meade, "Lock-in Amplifiers: Principles and Applications", P. Peregrinus, 1983.

15. H. J. Fischbeck and K. H. Fischbeck, "Formulas Facts and Constants for Students and Professionals in Engineering", Chemistry and Physics, Second Revised and Enlarged Edition, Springer-Verlag, 1987.

16. E. Voigtman and J. D. Winefordner, Prog. Analyt. Atom. Spectrosc., Vol. 19, pp. 7-143, 1986.

17. ORIEL Corporation, Light Sources, Monochromators and Spectrographs, Detection

Systems and Fiber Optics, Oriel Corporation, Stratford, CT, 1994.

18.   Model 1500SP/1702/1704 Instructions, 1973 SPEX Industries, Inc., Metuchen, NJ.

19.   Photomultiplier Tubes, Hamamatsu Photonics, K. K., Hamamatsu City, Japan, Jan/88.

20.   J. M. Stephens, Ph.D. thesis, in preparation.

21.   M. H. Hablanian, High Vacuum Technology, a Practical Guide, Marcel Dekker, 1990.

22.   R. E. Honig, RCA Rev., Vol. 23, No. 4 (1962).

Table I

Near resonances of SiO*(b$^3\Pi$ - X$^1\Sigma$) with Na 3s^{2}S - 4d^{2}D pump transition

Upper Atomic Level	SiO(v′, v″) b - X	$\Delta E(cm^{-1})^a$
Na 4d^{2}D$_{5/2,3/2}$	(1,0)	294
	(2,1)	45
	(3,2)	-209

a. Approximate value of molecular energy level minus atomic energy level. Positive denotes exothermic energy transfer.

Table II

Spontaneous emission rates, degeneracy factors, and energy increments for Na $4d^2D$ transition (from *Handbook of Chemistry and Physics*, 6th Ed.).

Transition	Energy (cm^{-1})	A value (10^7 s^{-1})	g_u	g_ℓ
$4d^2D_{5/2} - 3p^2P_{3/2}$	17575.375	1.2	6	4
$4d^2D_{3/2} - 3p^2P_{3/2}$	17575.41	0.21	4	4
$4d^2D_{3/2} - 3p^2P_{1/2}$	17592.606	1.03	4	2

Table III

Parameters relevant to the computation of source radiance.[a]

Wavelength (Å)	Photo-current (10^7 Å)	Photopic Response	PMT Radiant Sensitivity (mÅ/W)	Monochromator Transmittivity
5682.6	0.58	0.956	9.5	0.50
5688.2	1.0	0.956	9.5	0.50
5890.0	137[b]	0.768	6.7	0.48
5895.9	112	0.768	6.7	0.48

a. Lamp located immediately adjacent to monochromator entrance slit. Slit width set to 200 μ for resolution of ~ 0.16 angstrom.

b. Measured (not an equilibrium distribution).

Table IV

Estimated probe source flux and photocurrent at detector.

Slit Width	Geometric Extent (sr cm^2)	Estimated Radiant Flux (10^{-11} W)	Photo-current (10^{-8} A) predicted	Photo current (10^{-8} A) measured	Background (10^{-8} A)
250 μ	8 x 10^{-7}	0.72	4.4	1.88 ±0.02	0.10
1 mm	3.2 x 10^{-6}	2.9	18.2	9.74 ±0.05	0.12

Photocathode Radiant Sensitivity	Current Gain at 865 V	Solid angle Ω_F	Slit height
9.5 mA·W^{-1}	6.54 x 10^5	1.6 x 10^{-4} sr	2 mm

| Run | N$_2$O flow rate (gram/s) | Silicon | | Sodium | | P$_{bg}$[b] (mTorr) | P$_{Total}$[c] (mTorr) | Amplification Ratio[d] (AR) | Gain Coefficient[e] α(cm^{-1}) |
		oven current (Amps)	carrier gas (N$_2$) flow rate (gram/sec)	oven (nozzle) current (Amps)[a]	carrier gas (N$_2$) flow rate (gram/sec)				
Run 1	1.1 x 10^{-3}	650	$\leq$ 1 x 10^{-3}	5.2 (6.4)	$\leq$ 1.5 x 10^{-3}	50	~ 150	1.002 ± 0.004	4 x 10^{-4} ± 8 x 10^{-4} [f]
Run 2	2.7 x 10^{-3}	760	< 1 x 10^{-3}	5.7 (6.5)	< 1.5 x 10^{-3}	50	~ 250	1.0052 ± 0.004	1.04 ± 0.8 x 10^{-3}[g]
Run 3	6 x 10^{-4}	705	4.8 x 10^{-3}	5[i] (6.4)	1.4 x 10^{-2}	50	200	1.001 ± 0.002	3 ± 3 x 10^{-4}[g]
Run 4	< 1 x 10^{-4}	770	4.7 x 10^{-2}	5[i] (6)	< 1.5 x 10^{-3}	50	250	1.004 ± 0.002	9 ± 3 x 10^{-4}[g]
Run 5a	1.4 x 10^{-4}	830	3.4 x 10^{-2}[h]	5[i] (6)	< 1.5 x 10^{-3}	50	400	1.006 ± 0.002	1.3 ± 0.5 x 10^{-3}[g]
Run 5b	1.4 x 10^{-4}	820	3.4 x 10^{-2}	5[i] (6)	< 1.5 x 10^{-3}	50	400	1.008 ± 0.003	1.5 ± 0.5 x 10^{-3}
Run 5c	1.4 x 10^{-4}	795	3.4 x 10^{-2}	5[i] (6)	< 1.5 x 10^{-3}	50	400	1.007 ± 0.002	1.4 ± 0.4 x 10^{-3}
Run 6	8 x 10^{-4}	~780	5 x 10^{-3}	5[i] (6)	1.8 x 10^{-2}	40	200	1.003 ± 0.002	6 ± 4 x 10^{-4}

a See text for discussion.
b Background pressure.
c Total pressure with purge gases for self cleaning window and carrier gas flows.
d,e Based on data points determined from normalized data channel.
f Least squares analysis indicates positive gain with 70% confidence.
g Least squares analysis indicates positive gain with 90% confidence.
h Optical pyrometry indicates temperature ≥ 1700°C with no emissivity correction.
i Sodium oven current of 5 amperes corresponds to 530°C.

Appendix A

Transmissivity Through a Series of Polarizers

A polarizer transmits a polarized beam whose intensity is given by[1]

$$I = I_0((k_1 - k_2)\cos^2 \theta + k_2) \dots \tag{A1a}$$

$$= k \cdot I_0 \dots \tag{A1b}$$

The transmittance is k, k_1 and k_2 are the major and minor transmittances, respectively, and the angle θ corresponds to the angle between the polarization vector of the beam and the major polarization axis of the filter. A beam splitter preferentially transmits radiation polarized parallel to its plane of incidence. Conversely, horizontally polarized radiation will be reflected preferentially from the beam splitter.

The probe beam optical path (Figure A1) with a rotating polarizer situated between the two beam splitters can be understood, as a series of three polarizers. The first beam splitter (b_1) has its principal axis oriented horizontally, the second (the rotating polarizer) has arbitrary orientation of its principal transmission axis and the third (b_2) has its principal transmission axis oriented vertically.

The action of the linear polarizer can be expressed by[2]

$$K = \begin{bmatrix} k_1^{1/2} & 0 \\ 0 & k_2^{1/2} \end{bmatrix} \dots \tag{A2}$$

where the diagonal elements are the square roots of the principal major and minor transmittances, respectively. This expression is correct if the principal major axis is oriented in the x-direction. For an

31

arbitrary orientation, with the principal axis rotated through an angle θ with respect to the horizontal, the Jones matrix K' is given as

$$K' = R(\theta)\,K\,R(-\theta) \,... \tag{A3}$$

where the operator $R(\theta)$ is the rotation matrix,

$$R(\theta) = \begin{bmatrix} \cos\theta & \sin\theta \\ -\sin\theta & \cos\theta \end{bmatrix} ... \tag{A4}$$

The beam splitter b_1 acts as a horizontal polarizer, described by the Jones matrix H,

$$H = \begin{bmatrix} h_1^{1/2} & 0 \\ 0 & h_2^{1/2} \end{bmatrix} ... \tag{A5}$$

where $h_1 > h_2$ for horizontal polarization. Beam splitter b_2, which acts as a vertical polarizer, is described by the Jones matrix V,

$$V = \begin{bmatrix} v_1^{1/2} & 0 \\ 0 & v_2^{1/2} \end{bmatrix} ... \tag{A6}$$

where $v_2 > v_1$ for vertical polarization. The Jones matrix for the combination is then

32

$$J = VK'H\ldots \tag{A7a}$$

$$= \begin{bmatrix} J_{11} & J_{12} \\ J_{21} & J_{22} \end{bmatrix}\ldots \tag{A7b}$$

where the matrix elements are

$$J_{11} = v_1^{1/2}h_1^{1/2}(k_1^{1/2}\cos^2\theta + k_2^{1/2}\sin^2\theta)\ldots$$

$$J_{12} = v_1^{1/2}h_2^{1/2}(k_1^{1/2} - k_2^{1/2})\cos\theta\cdot\sin\theta\ldots$$

$$J_{21} = v_2^{1/2}h_1^{1/2}(k_1^{1/2} - k_2^{1/2})\cos\theta\cdot\sin\theta\ldots$$

$$J_{22} = v_2^{1/2}h_2^{1/2}(k_1^{1/2}\sin^2\theta + k_2^{1/2}\cos^2\theta)\ldots$$

These expressions represent an acceptable way to treat the power transmitted provided that, for the unpolarized light, there is no phase coherence between the two orthogonal components.[3] The amplitude of the beam is described by the Jones vector

$$\bar{A} = \begin{bmatrix} A_x \\ A_y \end{bmatrix} = \begin{bmatrix} 1 \\ 1 \end{bmatrix} \dots \tag{A8}$$

with transmission through the polarizer series given by

$$\bar{A}' = J\bar{A} \dots \tag{A9}$$

where the resulting elements of this vector are

$$A_1' = v_1^{1/2} h_1^{1/2} (k_1^{1/2} \cos^2\theta + k_2^{1/2} \sin^2\theta) + v_1^{1/2} h_2^{1/2} (k_1^{1/2} - k_2^{1/2}) \cos\theta \cdot \sin\theta \dots$$

$$A_2' = v_2^{1/2} h_1^{1/2} (k_1^{1/2} - k_2^{1/2}) \cos\theta \cdot \sin\theta + v_2^{1/2} h_2^{1/2} (k_1^{1/2} \sin^2\theta + k_2^{1/2} \cos^2\theta) \dots$$

The transmittivity is calculated as the ratio of the transmitted to incident irradiance (square of the amplitude)

$$k = \sqrt{\frac{\bar{A}' \cdot \bar{A}}{\sqrt{\bar{A}' \cdot \bar{A}}}} \dots \tag{A10}$$

Evaluating, these expressions one finds that the transmitted power is of the form

$$S = c_1 + c_2 \cdot \cos 4\theta + c_3 \cdot \sin 4\theta + c_4 \cdot \cos 2\theta + c_5 \cdot \sin 2\theta \dots \tag{A11}$$

where S corresponds to the signal and the coefficients can be calculated from the properties of the optical elements. However, the coefficients can also be determined from a least squares procedure using

evaluations from a series of angular position evaluations of transmission covering a large range of angle (usually for simplification of least squares expressions, the full rotation of the polarizer). With the coefficients determined, Equation A11 may be used to predict the expected signal for a series of angles that differ by small displacements, corresponding to small differences in attenuation. A rigorous test for sensitivity is afforded in this way. The signal level can be the demodulated voltage output from a lock-in amplifier, the normalized output for a dual beam experiment (Fig. A1), or the direct output for the probe signal for a single beam experiment.

A procedure can be implemented by employing a standard photographic polarizer. Data are collected over the full cycle of the trigonometric functions to simplify the appropriate expressions for the evaluation of c_1 to c_5 in equation A11. These are given for the configuration described in Figure A1 as

Table A1

Least-Squares Coefficients				
c_1	c_2	c_3	c_4	c_5
641.4629	-35.1775	39.5411	30.6040	-19.1863

Using the derived coefficients, one is able to generate the data exemplified in Table A2 where each signal level entry is an average of 100 data points and the uncertainty is the standard deviation (S.D.) of these 100 points. The average signal level is the average of the values in the corresponding signal level column. The error associated with each of these is the standard deviation of the mean.

Table A3 presents a comparison between predicted and measured values. An examination of the

35

data in Tables A2 and A3 suggests that the least squares procedure provides sufficiently good information so as to allow an estimate of the performance of the system described in Figures 2 and 3 of the text. For the configuration described in Figure A1, we note that the least squares prediction (S^{pred}) for the 32° and 34° positions indicates that rotating the polarizer from the 34° to the 32° position is equivalent to introducing an amplification of

$$AR = \frac{S^{pred}_{32°}}{S^{pred}_{34°}} = \frac{690.45}{687.91} \approx 1.004$$

Assuming a 5 centimeter gain length, amplification of this magnitude corresponds to a gain coefficient of approximately 8×10^{-4} cm^{-1}. Table A3 indicates that the measured value of this simulated amplification is

$$AR = \frac{S^{actual}_{32°}}{S^{actual}_{34°}} = \frac{691.5 \pm 2.0}{689.0 \pm 3.0} \approx 1.003 \pm 0.005$$

Although the uncertainty is of the order of the quantity that is being measured, the tabulated data suggests that one can distinguish between the two angular positions provided that several measurements are taken.

Table A3

Least-squares predictions of signal values and associated test data for test of sensitivity.

Angular Position	Least-Squares Prediction	Data	Error
32°	690.45	691.5	2.0
34°	687.91	689.0	2.99
36°	684.37	686.0	2.5
38°	679.87	682.0	2.4
40°	674.46	676.0	2.2
42°	668.21	668.9	1.9

Figure Captions

Figure 1:   Simplified diagram for sodium depicting levels relevant for proposed laser. 568.3 - 568.8 nm corresponds to region of $4d^2D$ - $3p^2P$ amplifier transition.

Figure 2(a):   Overhead view of reaction chamber with gain measurement system in place. Probe lamp is to upper right. See text for outline of propagance.

Figure 2(b):   Three dimensional closeup of mechanical chopper and beam splitter assembly following Figure 2(a).

Figure 3:   Schematic view of gain measurement assembly configured for dual beam experiment. Beam splitters are designated b_1 and b_2, lenses as l_1, l_2, and l_3, and mirrors as m_1 through m_5. See text for discussion of propagance.

Figure 4:   Configuration of silicon oven - SiO source and sodium source oven indicating also the reactant intersection region. See text for discussion.

Figure 5:   General scheme of dual beam spectrometry/radiometry system employing a single radiation detector and two lock-in detectors.

Figure 6:   Determination of geometric extent.
(a) Coupling from Na lamp into optical path
(b) Coupling through "pinhole" into monochromator slit aperature.
Drawing is not to scale.

Figure 7:   (a) Top view of Na-carrier gas nozzle assembly (the circular diameter is 5 in.) and
(b) side cutaway view of nozzle showing N_2O inlets, silicon oven configuration, and entrainment gas inlets.

Figure A1:   View of gain measurement optical train showing position of test polarizer. Beam splitters are designated b_1 and b_2, lenses as l_1, l_2, and l_3, and mirrors as m_1 through m_5. See also Fig. 3.
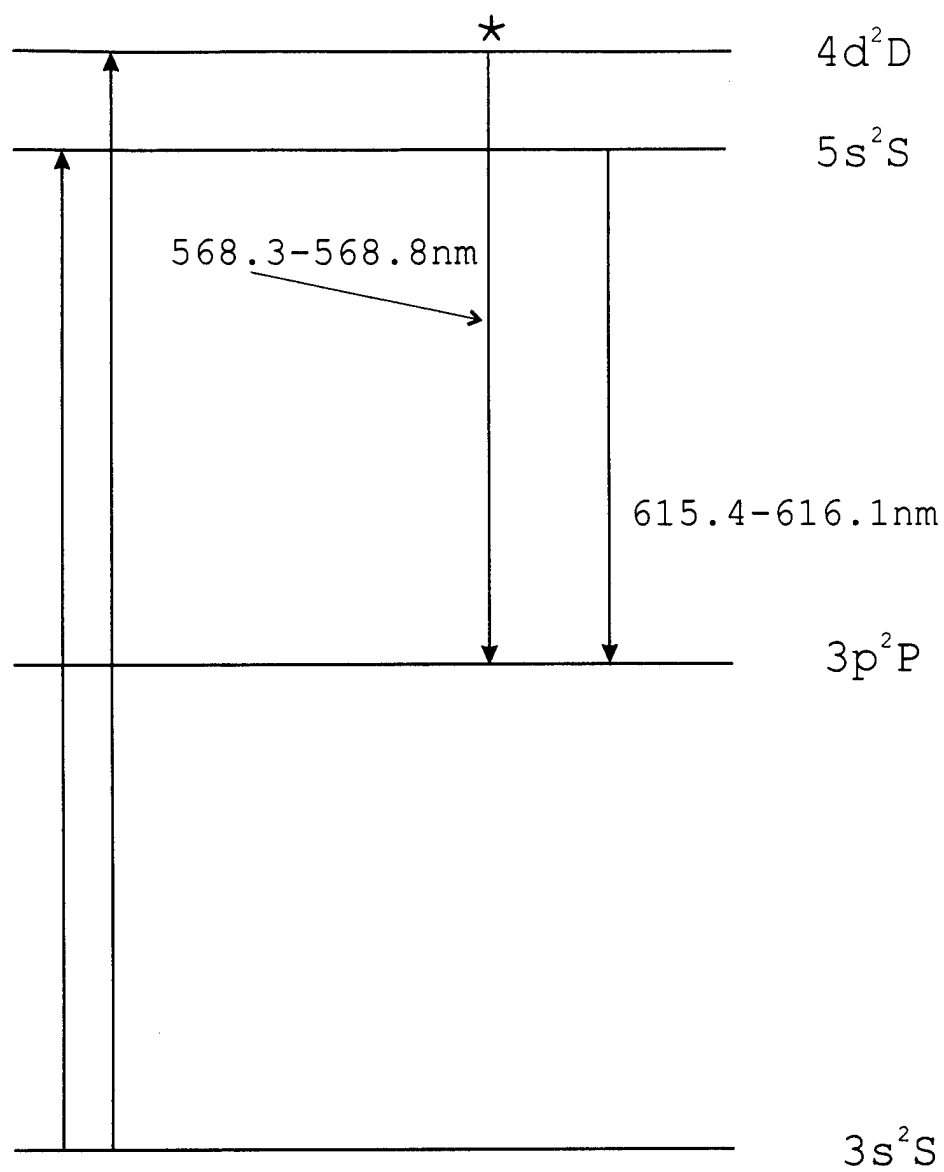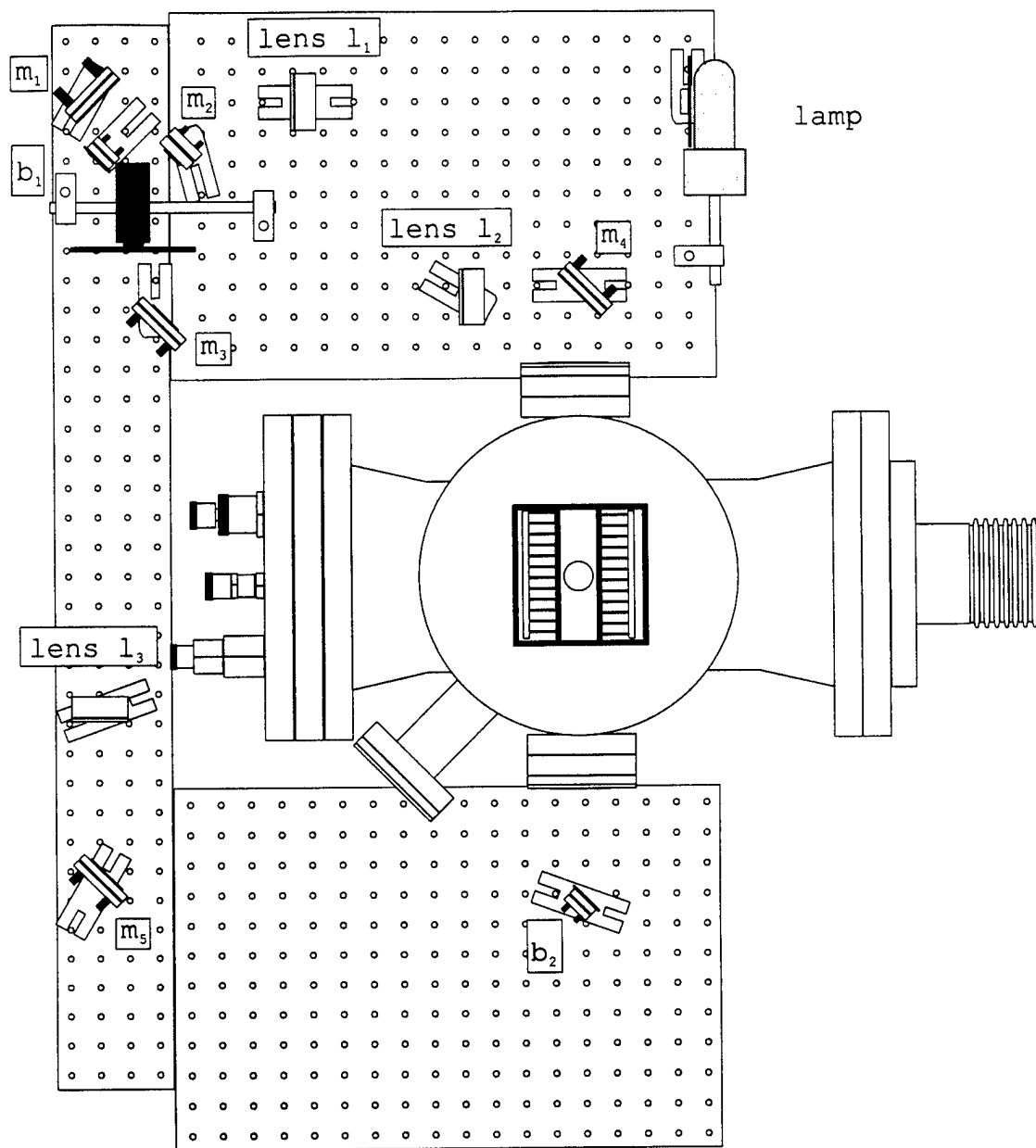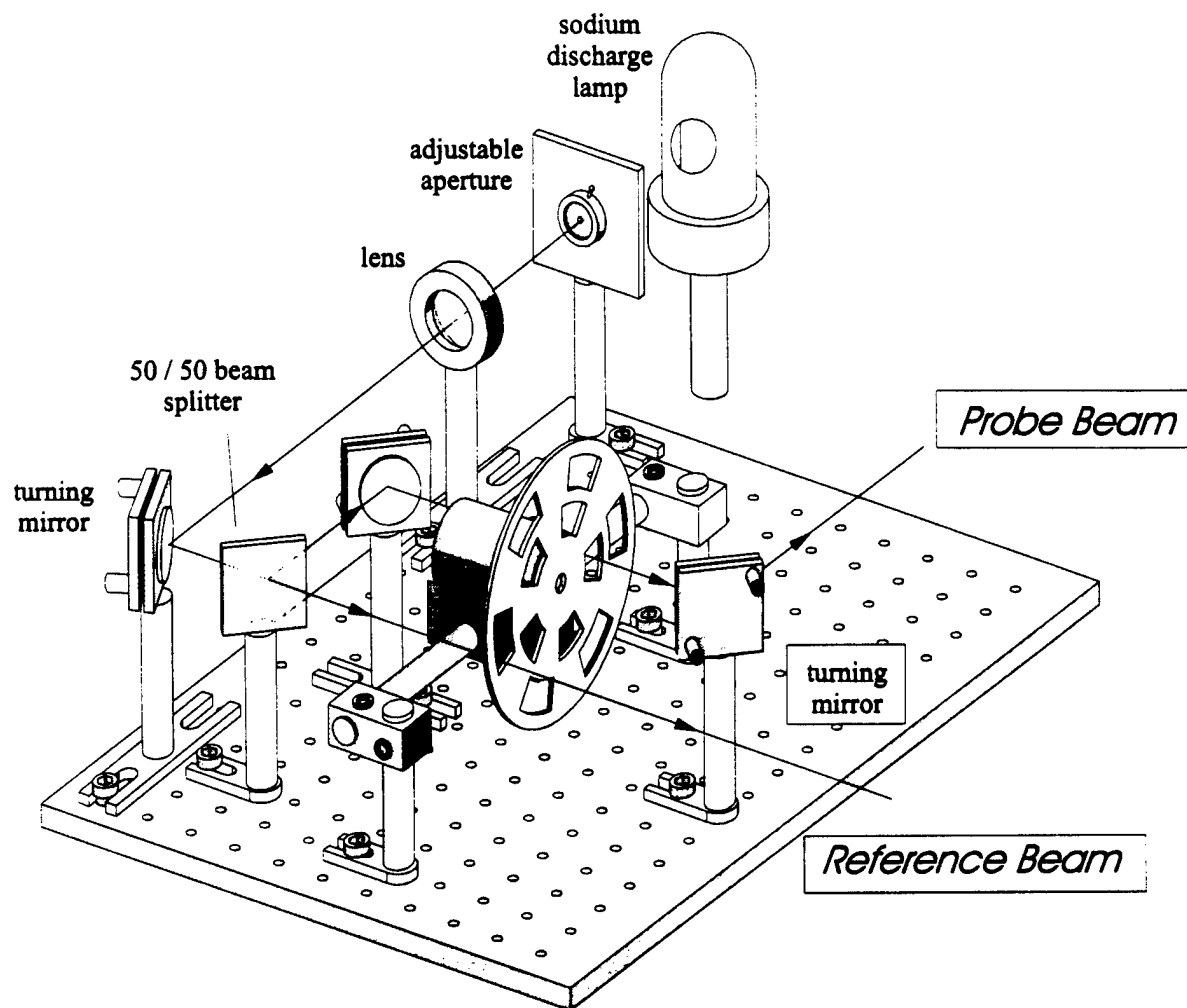
Figure 1

Figure 2(a)

Figure 2(b)

Three dimensional closeup of mechanical chopper and beam splitter assembly.

Figure 3

Relief Valve
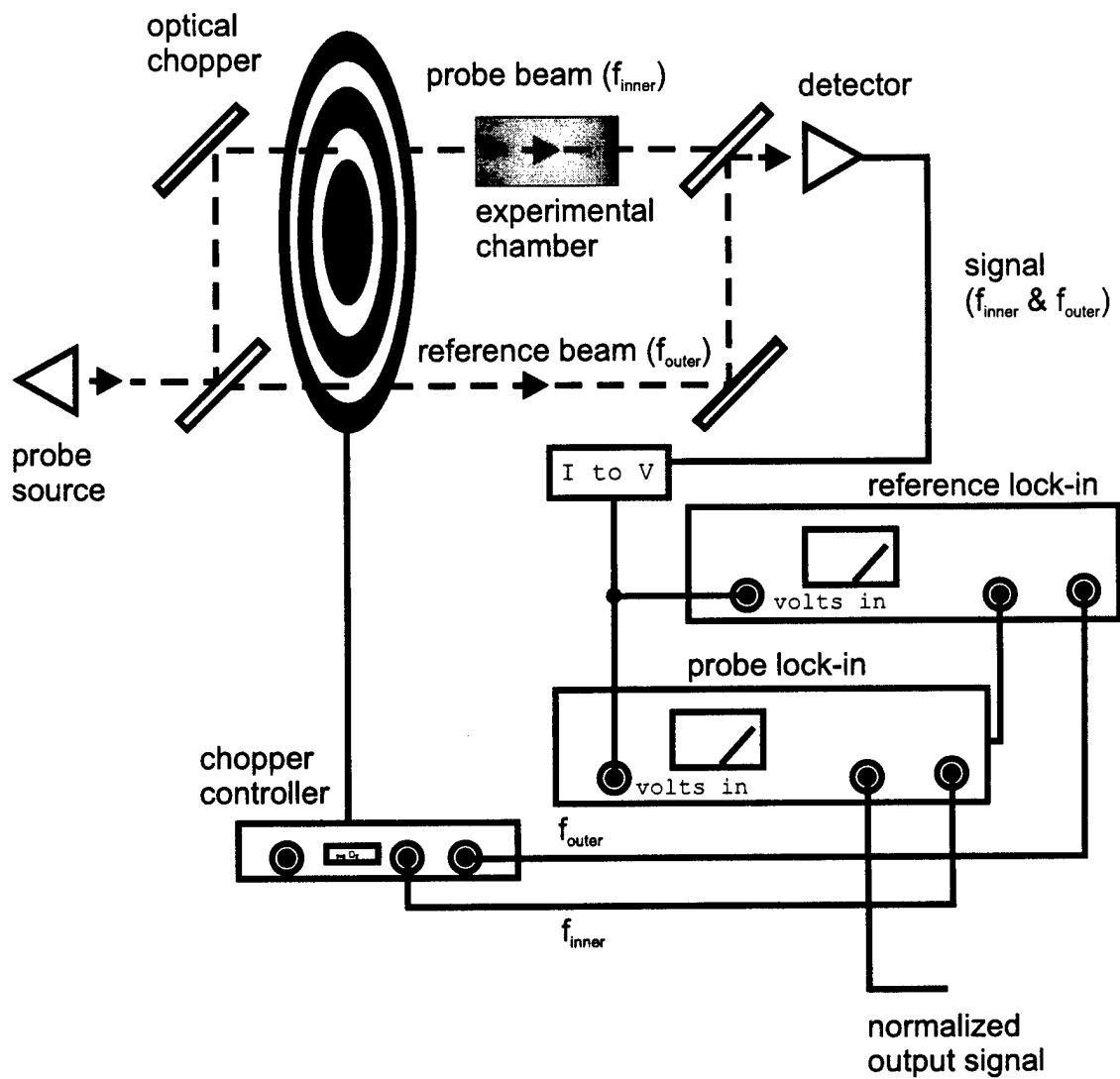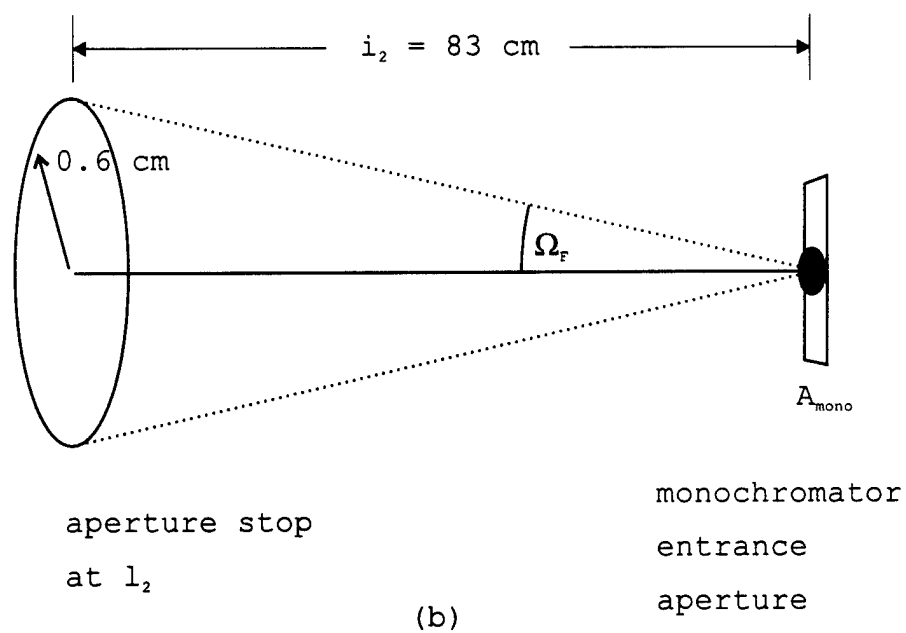
Thermocouple Gauge

18"

SiO Source Oven

Sodium Source Oven

Figure 4

optical
chopper

probe beam (f_{inner})

detector

experimental
chamber

signal
(f_{inner} & f_{outer})

reference beam (f_{outer})

probe
source

I to V

reference lock-in

volts in

probe lock-in

volts in

chopper
controller

f_{outer}

f_{inner}

normalized
output signal

Figure 5

$o_1 = 35.6$ cm

0.3 cm

0.6 cm

Ω_0

lamp
aperture

(a)

aperture stop
at l_1

$i_2 = 83$ cm

0.6 cm

Ω_F

A_{mono}

aperture stop
at l_2

(b)

monochromator
entrance
aperture

Figure 6

Silicon Oven Top

Outlet

(a)

Nozzle Array
(cut view)

Sodium and Carrying Gas

N_2O Carrying Gas (N_2) for silicon

(b)

Si   Zirconia
Felt   Zirconia
Collar

Water-Cooled Heat
Brass Jacket Reflector   Graphite
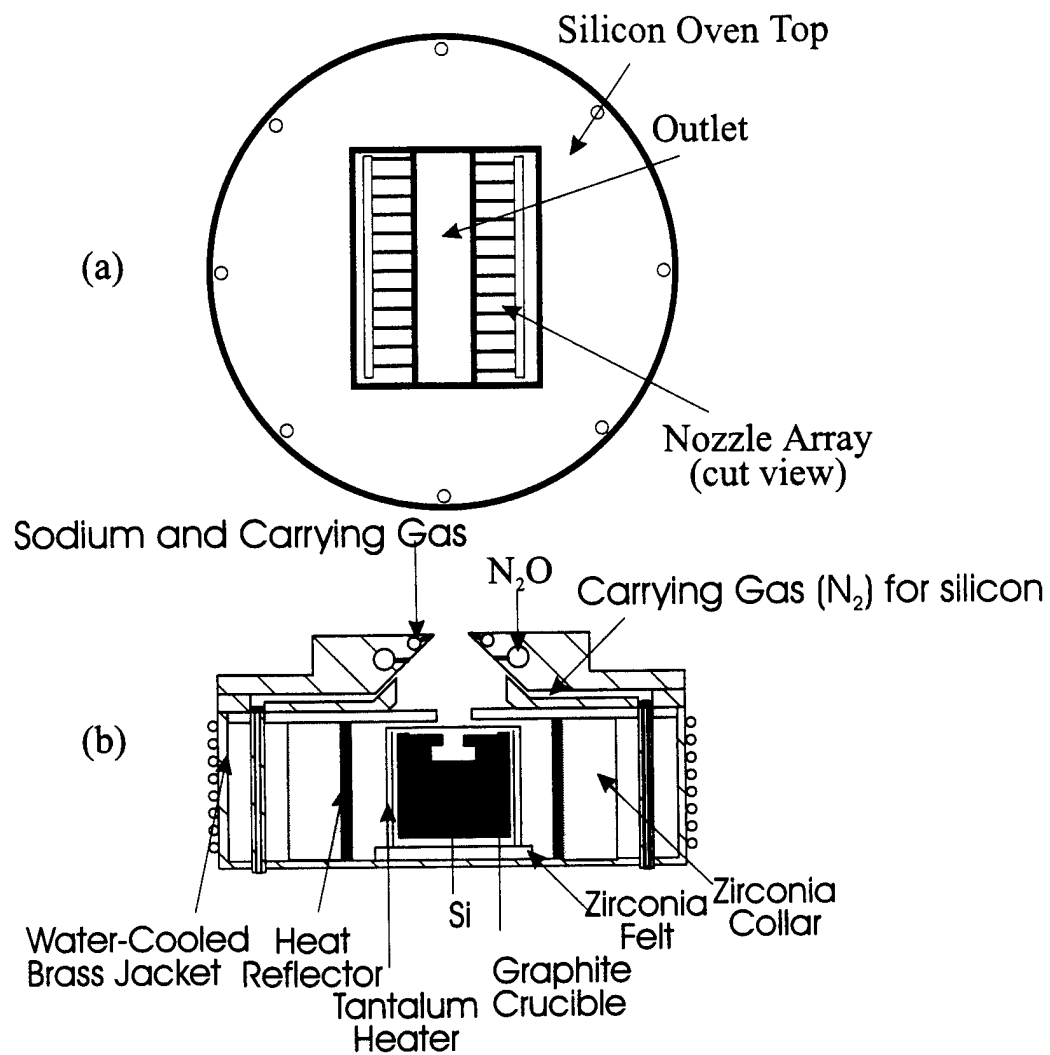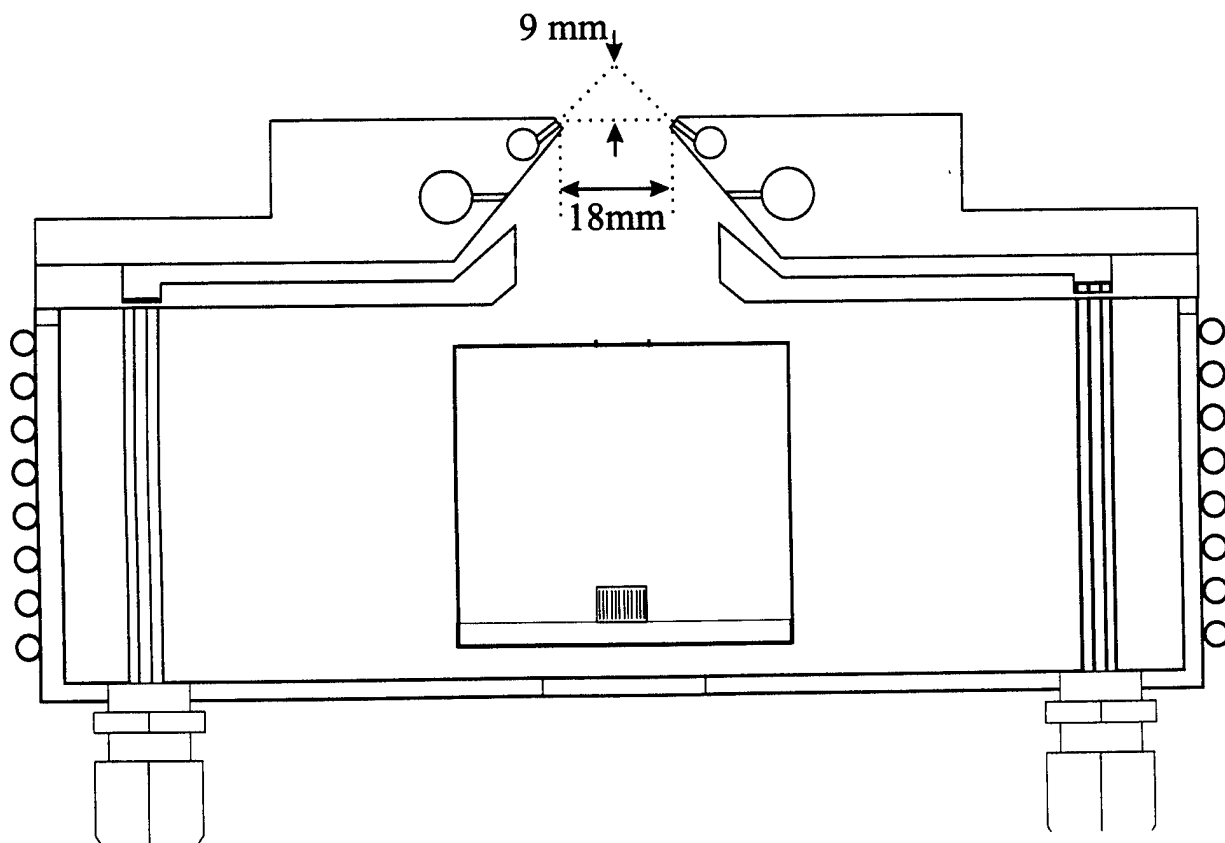Crucible

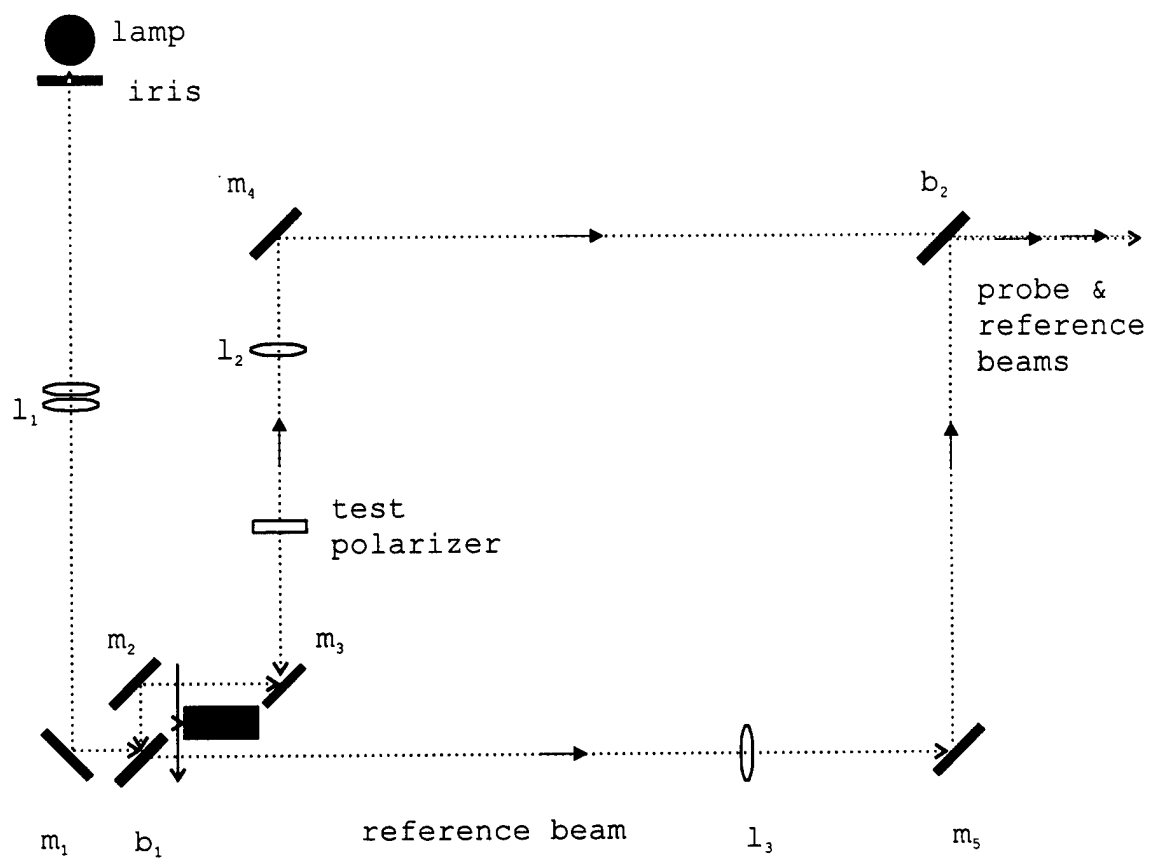Tantalum
Heater

Figure 7

9 mm

18mm

Figure A1

Appendix B

Rigrod Calculations - Estimating the Laser Output[1]

The potential output power, P_{out} was calculated commensurate with evaluated gains for the SiO-Na system according to Rigrod theory as,

$$P_{out} = I_{sat}A(1 - \alpha_{as} - \sqrt{(R_1 R_2)})(\alpha L_e + \ln\sqrt{(R_1 R_2)})/(1 - (R_1 R_2))$$

where I_{sat} is the saturation intensity, A is the cross sectional area of the gain medium, α_{as} is the distributed absorption/scattering loss coefficient, R_1 and R_2 are the mirror reflectivities, α is the zero power gain coefficient, and L_e is the effective gain length. Parameters used in the calculations were as follows:
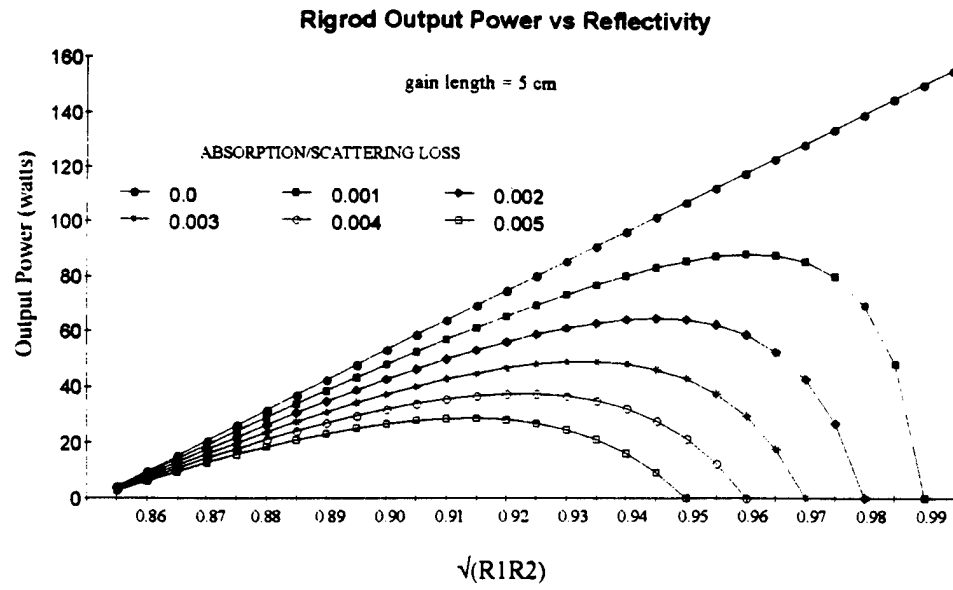
$$I_{sat} = 15,000 \; watts \, cm^{-2} \, for \; \alpha = 0.0005, 0.00071, 0.001 \; cm^{-1},$$
$$I_{sat} = 3,000 \; watts \, cm^{-2} \, for \; \alpha = 0.001, 0.003, 0.005, 0.0071 \; cm^{-1},$$
$$I_{sat} = 175 \; watts \, cm^{-2} \, for \; \alpha = 0.01, 0.05, 0.1 \; cm^{-1}.$$

Comparisons with the HF overtone system[1] as well as a-priori estimates[2] suggest, from the above parameterizations, that I_{sat} is in the range 60-6000watts/cm². The results of these Rigrod calculations for the geometry of a flow field consistent with the current reaction-energy transfer-stimulated emission zone are summarized in Table I with representative Rigrod curves in Figure B1. For the lower gains measured ($\alpha = 0.001 - 0.002$), with a set of 99.7% reflective mirrors in vacuum mirror mounts forming the laser cavity, we suggest a measurable laser output power of 1 to 10 Watts should be obtained. This should be compared to 1.6-2.0 milliwatts for spontaneous emission from the SiO-Na energy transfer reaction zone.
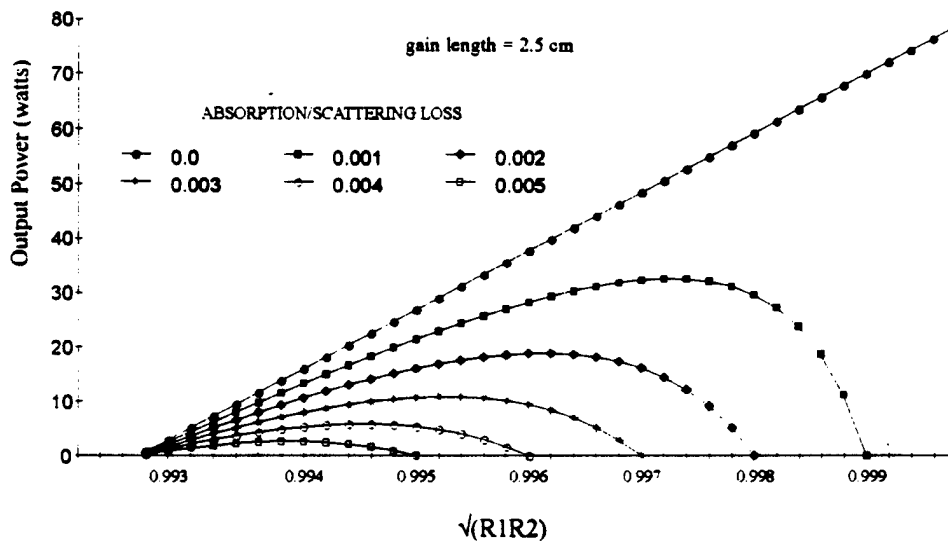
1.   Lee Sentman, University of Illinois, Urbana-Champaign, private communication and visits to the Gole Laboratory.
J. M. Stephens, J. L. Gole, L. H. Sentman, and M. Zaczek, "Potential for a Sodium Pumped Chemical Laser", 28th Plasmadynamics and Laser Conference, AIAA-97-2425, June 23-25, 1997.

2.   A. E. Siegman, Lasers, University Science Books, Mill Valley, California, 1986.

Table I
Rigrod analysis estimates of power for several estimates of gain coefficient.

	Output Power (watts)			
α (cm^{-1})	A, L$_e$, α_{AS} 3.6 cm^2, 5cm, 0.0025	A, L$_e$, α_{AS} 0.25 cm^2, 5cm, 0.0025	A, L$_e$, α_{AS} 3.6 cm^2, 2.5cm, 0.0025	A, L$_e$, α_{AS} 0.25 cm^2, 2.5cm, 0.0025
0.0005	0	0	0	0
0.00071	5	0.347	0	0
0.001	18/3.5	1.25/0.243	0	0
0.003	20	1.39	8	0.56
0.005	38	2.64	18	1.25
0.0071	55	3.82	27	1.875
0.01	≈13	0.903	≈2.5	0.174
0.05	≈65	4.51	≈33	2.29
0.10	≈100	6.94	≈55	3.82

Rigrod Output Power vs Reflectivity

Rigrod output power for $\alpha = 0.003$ cm^{-1}, $I_{sat} = 3000$ W cm^2, A = 3.6 cm^2 for gain length (a) $L_e = 5$ cm and (b) $L_e = 2.5$ cm.

Figure B1

Appendix C

Details of Alignment Procedure for Lasing Demonstration

The following discussion refers to the schematic diagrams corresponding to Figures 4-7 of the main report. The alignment procedure involves first the overall system alignment using the He/Ne laser (Fig. 4). This is followed by translation stage, reaction zone, and laser mirror and/or fiber optic alignment.

Alignment of system with He/Ne laser (refer to Figures 4,7)

1. The He/Ne laser is first collimated with lenses and routed along the longest possible path around the vacuum mirror mount chambers and reaction zone region.

2. A semitransparent paper target is placed at the far port of the reaction chamber just inside the vacuum mirror mount chamber. The scattered laser light from the He/Ne laser fills the 1 1/8" orifice (Figure 7) which coincides with a 1 1/8" outer ring on the paper target. Alignment of the orifice light scatter and target places the center of the target at the center of the chamber port.

3. An aluminum disk insert target is inserted in the near port of the reaction chamber, tightly collimating (selecting) the light from the He/Ne laser beam. Laser light passing through a pinhole centered in the aluminum target will now form a small dot on the semitransparent target.

4. The final steering mirror preceding the near stage vacuum mirror mount is adjusted so as to place the laser output beam at the center of the aluminum target.

5. The second to last mirror stage is subsequently adjusted so as to place the He/Ne laser beam in the same relative position that it appears to occupy on the semitransparent target.

The final mirror stage is again adjusted so that the He/Ne laser beam is centered at the pinhole opening in the aluminum target and the beam position on the semitransparent target is evaluated. The process is repeated until the He/Ne laser beam passes both through the center of the aluminum and semitransparent targets.

6.   The He/Ne laser and system are now aligned, the aluminum and semitransparent targets are now removed, and the remaining alignment will be done relative to the He/Ne laser beam.

Translational stage alignment (Figure 4)

The procedure is first carried out with the far stage and then applied to the near stage.

1.   An Al target with centered pinhole orifice is placed into the translational stage and rotated until it is roughly perpendicular to the alignment beam.

2.   The stage is then translated until the Al target is centered with the beam.

(It is important that the stages be regularly exercised to prevent buildup of sodium or dust particles in their translation mechanism.)

Reaction Zone alignment (Figures 5,6)

1.   After the silicon and sodium nozzle assemblies are initially placed into the reaction-energy transfer chamber configuration (Figs. 5,6) an aluminum block target with pinhole channel is clamped into the top outlet (Na nozzle assembly). If the reaction chamber configuration is correctly aligned, the beam will pass directly through the Al block alignment device. Otherwise, the system can be adjusted by moving the silicon support base up and down, moving the system from side to side as the Na carrier lines moving in the same direction,

or rotation with the Na lines moving in opposite direction.

Fiber Optic alignment (Figure 4)

1. Remove the lens positioned before the fiber optic and adjust its mirror to center the laser on the fibers.

2. To image the sodium lamp, place it in the beam path allowing for lamp warm up.

3. Position the fiber optic lens so that the fiber is at the lens focal length while the light from the lamp is still centered. The fiber optic itself, mounted on a translation stage, is also be adjusted.

Laser Mirror alignment (Figure 4)

The procedure is again first carried out with the far stage and then applied to the near stage. The procedure is designed to incorporate the glass window located at the steering mirror side of the vacuum mirror mount chamber.

1. The mirror placed in the far stage is rotated to observe the reflected light from the aligned (system) He/Ne laser and adjusted until the laser beam reflects back on itself within the vacuum mirror mount box-reaction chamber configuration.

2. The reflected beam in (1) is then centered onto the iris located directly in front of the alignment laser.

3. It is to be noted that the back surface of the near mirror is used for its alignment. This surface, however, is very nearly parallel with the front surface at the mirrors center.

After this procedure, the final alignment mirror, 4, can be removed and replaced by a

cinder block placed in front of the power meter. Similarly, a cinder block is placed in front of the fiber optic. The cinder block in front of the power meter is removed and replaced for each measurement during a run.